PHILOSOPHICAL TRANSACTIONS OF THE ROYAL SOCIETY A MATHEMATICAL, PHYSICAL & ENGINEERING SCIENCES

The Impulse Breakdown Voltage and Time-Lag Characteristics of Long Gaps in Air. I. The Positive Discharge

R. T. Waters and R. E. Jones

Phil. Trans. R. Soc. Lond. A 1964 **256**, 185-212
doi: 10.1098/rsta.1964.0003

THE IMPULSE BREAKDOWN VOLTAGE AND TIME-LAG CHARACTERISTICS OF LONG GAPS IN AIR
I. THE POSITIVE DISCHARGE

By R. T. WATERS* and R. E. JONES†

Research Laboratory, Associated Electrical Industries, Aldermaston Court, Aldermaston, Berkshire

(*Communicated by T. E. Allibone, F.R.S.—Received* 30 *January* 1963)

[Plates 3 to 9]

CONTENTS

The electrical breakdown of rod/rod, rod/sphere and rod/plane gaps in the atmosphere has been examined oscillographically and photographically. Positive polarity impulse potentials of crest value up to 1 MV, of wave-front variable between 0·06 and 2·0 μs and of wave tail 2 ms were used. It has been found that the lack of a sharply defined breakdown potential was due to the existence of long time lags quite distinct from the shorter times to breakdown observed with the conventional short wave-tail impulse. A 'dead-time' of low probability of breakdown on the wave tail separated the two classes of breakdown.

The breakdown voltage of a rod/rod gap has been found to be dependent upon the wave front of the impulse. An accompanying photographic examination of the initial corona phase of breakdown also revealed a variation with the impulse voltage wave front. It is shown that these results were consistent with the electric field distortion arising from space charge. The corona phase of breakdown was responsible for this space charge. The statistical behaviour of long gap breakdown

* Now Senior Lecturer in the Department of Electrical Engineering, Welsh College of Advanced Technology, Cathays Park, Cardiff.

† Now at Elliott Bros (London) Ltd, Elstree Way, Borehamwood, Hertfordshire.

was due to random variations in the corona phase. The effect of the statistical time lag in the production of initiatory electrons upon the corona phase is discussed.

A rotating-mirror camera of $f/1{\cdot}0$ aperture and a technique for controlled suppression of the breakdown enabled the growth of the discharge with time to be studied in some detail. It was shown that the positive leader either preceded or was coincident with the negative leader, depending upon the gap arrangement. It is concluded that the establishment of the leader at the high-tension electrode is the criterion for breakdown. The role of the earthed cathode in aiding this leader development was dependent upon its size and geometry. For cathodes of small dimensions the occurrence of a negative corona phase increased the anode electric gradient; for large cathodes the surface charge induced by the anode corona discharge became important. The variation of breakdown strength with gap geometry is accountable in these terms.

1. Introduction

When impulse voltages are applied to long gaps in which the electric field is not uniform, the breakdown process in air consists of three main stages: corona development at the electrode of higher electrical stress, the formation of leader channels proceeding across the gap, and the main stroke formed by the discharge of available energy through one of the leader channels. The criterion for breakdown is the formation of a stable leader channel succeeding the corona stage.

The 'time lag' to breakdown is usually defined as the time to the occurrence of the main stroke, and is the sum of the time taken for a leader to be initiated, and the time it takes to travel across the gap. In strongly inhomogeneous fields the corona stage occurs rapidly upon voltage application so any statistical time lag arising from a lack of initiatory electrons is small; the total time lag is therefore substantially the time taken for the leader to cross the gap, and is called the formative time lag.

In the work to be described, this simple subdivision of time lag into statistical and formative components is found to be less apt than hitherto considered, since ionization processes in long gaps have been found to be almost completely suppressed for long periods of time. The term 'dead-time' will therefore be used to describe the time lag between the statistical time lag and the true formative time lag. Long dead-times have been encountered in the present work because impulse voltages having very long wave tails have been used.

The breakdown process has been studied oscillographically by measurement of the voltage across the gap and the current flowing in it, and with the aid of rotating cameras. Several electrode configurations have been studied and the paper reports the results obtained with a positive potential applied to the high-voltage electrode. A further paper will describe the breakdown process with a negative potential.

Several factors influence the time lag, apart from the statistical time lag; these are the electric gradient, the circuit resistance, the electrode geometry and the influence upon the field of surrounding objects. Earlier work by Allibone & Meek (1938) and Stekolnikov & Bagirov (1954) dealt with some of these effects; however, voltages were applied in excess of the minimum voltage required to break down a gap, and in general the leader stroke started from the anode before the crest of the impulse voltage had been reached. In the present work the long dead-times referred to have been found to disappear when voltages sufficiently in excess of the minimum breakdown voltage were applied, and when wave

tails of shorter duration (and therefore necessitating higher voltages to cause breakdown) were used. There are, however, many anomalies which will be discussed.

In Allibone & Meek's work large series resistance was used in circuit to reduce the main stroke current and so avoid the fogging of the rotating-film camera records of the leader stroke by the strong light from the main stroke; unfortunately a large series resistance reduces the rate of rise of voltage in the gap and complicates the interpretation of the breakdown process. In the present work this complication was avoided and all records were taken with low series resistance and with impulses of short wave front.

When the leader channel is well established, breakdown inevitably results provided that the potential difference is maintained across the gap. In inhomogeneous-field gaps the conditions required for the formation of a leader channel are unknown, and thus no theoretical means exist for estimating breakdown voltages in these gaps. The appearance of the leader channel has seemed to occur randomly in time, which suggested that the detailed study of times to breakdown in long gaps might be unrewarding (Loeb 1959).

The present investigations show that well-defined patterns occur in the time-lag behaviour of long sparks; the form of these patterns is solely due to variations in the time of appearance of the leader and not to variations in the leader velocity.

The consequences of these results, of part of which a summary has been previously communicated (Waters & Jones 1959), are twofold: first, the breakdown voltage characteristics of long gaps can be related to time-lag observations, since these determine whether breakdown occurs under transient voltages; secondly, the gap conditions likely to lead to the successful initiation of the leader stroke can be examined.

2. Experimental methods

(*a*) *Impulse generator*

For much of the work a six-stage impulse generator of maximum output 1·0 MV, discharge capacitance $2{\cdot}17 \times 10^{-9}$ F and distributed resistance 300 Ω was used. The output wave form as defined by British Standard 923 (1940) was normally 0·5/2000 μs, the wave-front circuit consisting of a $2{\cdot}17 \times 10^{-10}$ F capacitor connected to the impulse generator through a resistor of 500 Ω. This capacitor also served as the high-voltage component of a potential divider connected to a high-speed oscillograph. The wave front could be reduced to a minimum value of 0·06 μs by reducing the value of the series resistance and diminishing the inductance of the circuit; when the wave fronts were very short the wave tail was 3500 μs. The gap under study was connected directly in parallel with the wave-front capacitor.

All breakdown voltage measurements were corrected for variations in atmospheric density in accordance with B.S. 358 (1960). Over a long period of observation the maximum spread of results due to humidity variations was merely ±1%. Consequently no account of this variable was taken.

(*b*) *Gap geometry*

It was known from earlier work that the geometry of the gap has a large influence on the nature of the discharge. The extreme conditions are achieved with one electrode pointed and the other an infinite plane. Instead of a pointed electrode, however, a 1·9 cm diameter

rod was used with its end made hemispherical, as this geometry has the advantage that prior to initial breakdown of the gas the electric field between the electrodes can be computed.

The plane electrode was constructed from 16 s.w.g. aluminium sheet. A 6 ft. by 6 ft. flat surface was bounded by a cylindrically curved edge of radius 6 in. The corners were of radius 15 in. For the range of spacings employed this was sufficient to prevent discharges to the perimeter of the electrode.

The electric field at all points in a gap between such electrodes was determined by means of a resistor network analogue, account being taken of the presence of the walls, floor and ceiling of the laboratory. The axis of the gap was vertical, the height of the mid-point being 2 m above ground.

Rod/rod electrodes are commonly used in engineering for lightning protection on many forms of insulation and in some testing procedures. Observations were made on such gaps, including those composed of square-section rods cut square at their ends, following engineering practice. It is for gaps of this sort that much of the published data have been obtained (American I.E.E. Standard no. 4, 1940).

(*c*) *Time-lag observations*

The influence upon times to breakdown of gap size, crest voltage and wave form of the applied impulse were investigated; records were made in the form of histograms of N_t against t, where N_t was the number of breakdowns to occur at a time t following application of the impulse potential. Such distributions were constructed from sets of 10, 25, 50 or 100 impulses. Despite the statistical nature of the data and the influence of atmospheric conditions on breakdown levels a large accumulation of data confirmed that the general characteristics of the time to breakdown were remarkably reproducible. Over 25 000 discharges were examined oscilloscopically.

(*d*) *Photography of the discharge*

The time-lag and breakdown voltage data were augmented by stationary and time-resolved photographic recording of discharge growth. An $f/1{\cdot}0$, 61 mm lens was designed for this work (Dyson, Hemmings & Waters 1960) which was found considerably superior to any available quartz lens. It was used in conjunction with a rotating mirror housed in a vacuum chamber. At a mirror speed of 30 000 rev/min an image speed of $0{\cdot}35$ mm/μs resulted.

The high aperture of this lens and its transparency to ultra-violet radiation enabled the faint early stages of breakdown, especially the impulse corona, to be recorded without difficulty. When the voltage was insufficient to cause flashover of the gap, no precautions to prevent fogging of the film were necessary. With higher voltages a technique was adopted to avoid the fogging of the film by light from the main stroke, the spark being suppressed in its later stages by means of the discharge of the impulse generator through a 75 cm diameter sphere gap. The large variations in time lag of the long spark at low overvoltages made a predetermined chopping time of little use. Instead, a circuit was devised which ignited the sphere/sphere gap at any desired stage of discharge growth in the test gap, whatever the total time lag of breakdown (Waters & Jones 1962).

PHILOSOPHICAL TRANSACTIONS OF THE ROYAL SOCIETY A MATHEMATICAL, PHYSICAL & ENGINEERING SCIENCES

3. Results

(*a*) *The corona discharge from a rod anode*

Discharges in grossly inhomogeneous fields are initiated by a corona discharge in the region of greatest electrical gradient. It is convenient for discussion that the description of the breakdown of long gaps which follows be prefaced by an examination of the corona discharge at the high voltage electrode when spaced at a greater distance from a plane cathode than the sparking distance.

The corona discharge from a rod anode consists of numerous channels occupying a roughly hemispherical volume centred at the tip of the electrode, as shown in figure 1, plate 3. These records will be discussed in Appendix I, where the effect of impulse wave front and crest voltage upon the corona structure is described. It is useful here to contrast the narrow corona channels in figure 1(*c*) with the broader channels of figure 1(*d*) which were obtained with identical impulses, since these will later be shown to have a differing influence on the later stages of the breakdown of long gaps.

A crest voltage of 90 kV caused corona discharge to occur on 50% of the applied impulses. At this voltage the length of the corona channels was 4 cm. Photographic measurement of the radius of the discharge volume, produced by impulse potentials of 0·50 μs wave front, showed that this increased linearly with crest voltage at 0·145 cm/kV. The radius was not strongly influenced by the rod/plane gap spacing, and upon reduction of the gap to the sparking distance the corona discharge traversed two-thirds of the gap. For gaps shorter than 100 cm in length, a further faint discharge was observed between the corona boundary and the plane at the breakdown voltage.

The velocity of propagation of the corona channels from a rod electrode at 1 MV (which produces a corona discharge of length 130 cm) has been measured by two methods (Waters & Jones 1961). The velocity was found to be uniform throughout the corona growth, with a value of 1×10^8 cm/s.

The current flowing in the earthed plane electrode during the application of the impulse potential wave front is a displacement current resulting both from the charging of the gap capacitance to the peak voltage and from the net charge deposited into the discharge space during the corona growth. This total current was measured oscillographically for an impulse potential of 1 MV peak and 0·50 μs wave front. Integration of the current passing to earth during the development of the corona discharge indicated a total charge flow of 14 μC.

Further measurements of the charge flow were made by recording the voltage developed across a 0·53 μF capacitor placed in series with the plane electrode. For a rod/plane separation of 200 cm, the capacitor voltage was found to increase approximately as the square of the potential difference applied to the gap. Since the component of displacement current resulting from the charging of the inter-electrode capacitance would be linearly proportional to the potential difference, the observed increase indicated that this was small compared with the component associated with the corona discharge. The charge deposited on the signal capacitor at a gap voltage of 1 MV was 14·5 μC. The length of the vertical rod electrode for this gap was 30 cm. A capacitance to earth of 0·1 pF per centimetre of the rod would result in 3 μC of charge being distributed on the rod at this applied voltage.

PHILOSOPHICAL TRANSACTIONS OF THE ROYAL SOCIETY A MATHEMATICAL, PHYSICAL & ENGINEERING SCIENCES

The corona discharge at 1 MV therefore produces a space charge of about 11·5 μC in the space it occupies.

(*b*) *Rod/rod gaps*

(i) *Breakdown voltages and time-lag variation with gap length*

Impulses of 0·5/2000 μs were applied to gaps composed of hemispherically tipped rods. The critical voltages found to result in 0 and 100% breakdown of the gap are shown in figure 2, together with previously published results for 1·0/50 μs impulses (Allibone 1937) and 60 c/s potentials (American I.E.E. Standard no. 4, 1940).

Figure 3 shows a typical selection from the time-lag measurements obtained. The important feature of these histograms is that for many gap lengths two classes of breakdown were observed, namely those of short time lag (< 20 μs) and those occurring after considerable delay (> 70 μs). Over a range of voltage levels both types occurred together, with no time lags of intermediate duration being recorded.

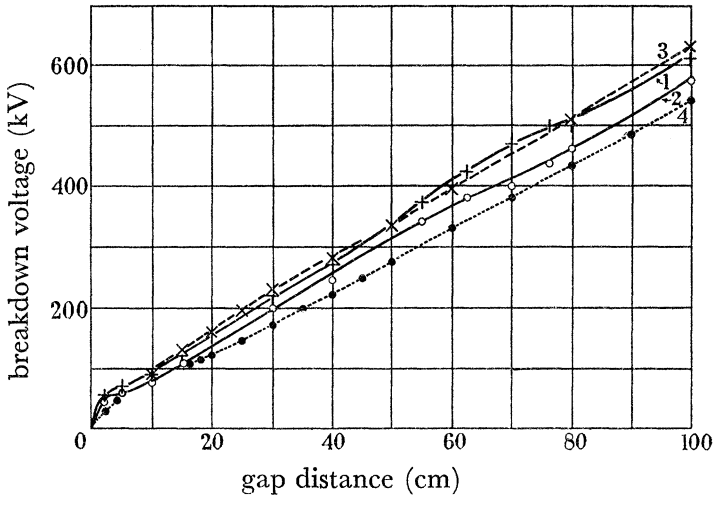

FIGURE 2. Breakdown voltages for rod/rod gaps. Curve 1, 100% breakdown, 0·50/2000 μs wave; 2, 0%, 0·50/2000 μs; 3, 50%, 1/50 μs (Allibone 1937); 4, 60 c/s a.c. breakdown (A.I.E.E. std. no. 4, 1940).

Higher voltages served to increase the number of short time lags at the expense of the long time-lag population.

For gaps longer than 40 cm the probability of occurrence of long time lags decreased with increasing gap distance; they became rare at 70 cm and absent at greater distances.

This change was accompanied by unstable behaviour which was especially severe for a 55 cm gap, for which no characteristic histograms could be obtained. Either short or long time lags appeared in long sequences, rather than with a pulse-to-pulse probability solely determined by the applied voltage.

(ii) *Time-resolved photography*

40 cm *gap*. Discharges initiated by impulses of wave front 0·50 μs, but arrested before completion, were photographed with the $f/1{\cdot}0$ streak camera. At a voltage level of 275 kV the breakdowns obtained were mainly of long time lag, and a typical record is shown in figure 4 (*a*), plate 4. The time lag was 160 μs, and the image speed on the film was

0·07 mm/μs. This photograph shows that throughout the dead-time no visible discharge occurred in the gap, despite the maintained potential difference across it. An energetic discharge of corona channels occurred at both the high-tension and earthed rods very shortly after the impulse voltage was applied to the gap. No time difference could be measured between these discharges. Leader channels developed from both the anode and

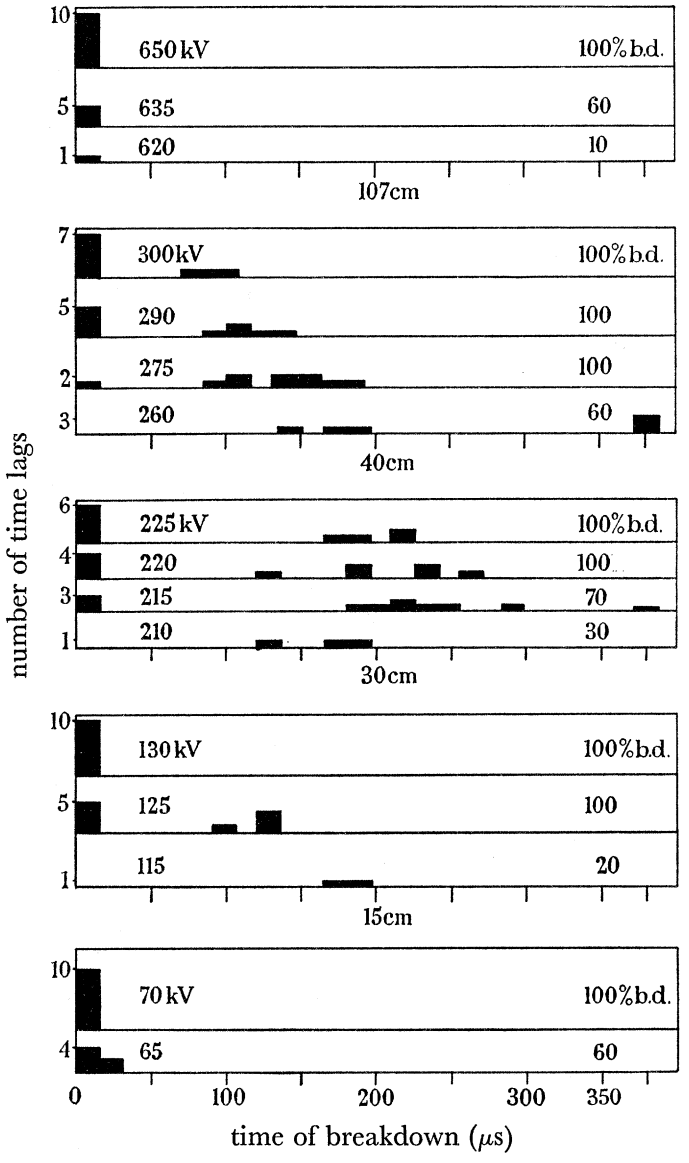

FIGURE 3. Time-lag histograms for rod/rod gaps subjected to 0·50/2000 μs impulses for increasing voltage levels.

cathode following the dead-time, accompanied by the dense envelope of glow discharge which has been described by previous workers (Allibone & Meek 1938; Komelkov 1947; Saxe & Meek 1955), but which the present camera records more strongly than hitherto. When the discharge is arrested before completion the track which has been established by the leader phase is re-illuminated along its whole length. This is a high-speed process, and results in a V-shaped appearance on the time-resolved photograph.

Figure 4 (*b*) is an example of the few short time-lag breakdowns obtained at this voltage. In this case the leader channels developed without interruption following the initial corona burst. A clear difference from the breakdowns of long time lag lay in the structure of the corona channels. Whereas the long time-lag breakdown of figure 4 (*a*) followed corona channels of the broad structure described in § 3 (*a*), the breakdown of figure 4 (*b*) was preceded by a narrow-channel corona. In 17 applied impulses, only two breakdowns of short time lag occurred. These were also the only discharges exhibiting the narrow-channel corona.

Figure 4 (*c*) is a record obtained where no sparkover resulted from the application of the impulse wave. The anode and cathode corona near time zero were as extensive as in a discharge resulting in long time-lag breakdown.

A higher image speed of 0·31 mm/μs was used to examine the leader channel growths more closely. Figure 4 (*d*) shows a breakdown of time lag 90 μs; the time resolution was such that the initial corona discharge was not recorded on the photographic negative. It is clear from this record that the anode leader began to propagate about 2·1 μs before the cathode leader was formed.

Upon raising the applied voltage to 310 kV to ensure a high proportion of sparks of short time lag, the discharge appeared as in figure 4 (*e*). Here the leader development from each electrode appeared to be simultaneous. At this higher voltage the breakdown was of short time lag even when the anode corona was of broad-channel structure.

55 cm *gap*. Figure 5 (*a*), plate 5, is a photograph of a breakdown of 7·0 μs time lag in a 55 cm rod/rod gap, obtained with an image speed of 0·31 mm/μs. The impulse potential was of 380 kV crest and 0·50 μs wave front. At the breakdown voltage across this gap distance it was invariably found that two corona bursts occurred at the cathode. The first and smaller burst took place near time zero, and was followed after about 1·8 μs by a stronger discharge. Even in the case where flashover does not occur, the second cathode discharge was shown to be present (figure 5 (*b*)). The corona phase of figure 5 (*a*) is of narrow structure; this was found to be the case in 11 out of the 35 discharges photographed, and all 11 resulted in short time-lag breakdown. In the remaining 24 discharges exhibiting the broader corona channels, 7 resulted in short time-lag breakdown (figure 5 (*c*)), 3 in long time-lag breakdown and 14 failed to attain sparkover.

The anode leader channel was found always to be well developed before the cathode leader was initiated.

170 cm *gap*. A time-resolved photograph of the arrested breakdown of a 170 cm rod/rod gap is shown in figure 6, plate 6. The crest voltage was 970 kV and the wave shape 0·50/2000 μs. The impulse corona at the high-tension anode was extensive and consisted of numerous narrow channels. The initial corona discharge at the cathode surface was small, followed at 2·9 μs interval by a second discharge. The negative leader was then initiated, after which the luminosity of the positive leader already developing was increased.

(iii) *The effect of impulse wave front on breakdown voltages and time lags*

A series of impulses of fixed crest value but of variable wave front was applied to a 76·2 cm (30 in.) gap between hemispherically ended rods. A typical curve showing the

variation of percentage breakdown with wave front is given in figure 7. It is seen that the discharge underwent a sharp decrease in breakdown probability for the faster wave fronts.

Measurements of breakdown voltages and time lags for fast wave fronts were carried out for the three gap lengths 30, 52·5 and 70 cm.

Figure 8 illustrates the variation of the two breakdown voltage levels with wave front, these levels being (*a*) the voltage required to yield 50% breakdown of the gap, irrespective of time lag, and (*b*) the voltage required to ensure that 50% of the breakdowns are of short time lag. It is (*b*) that would define the breakdown level for an impulse with the conventional wave tail of 50 μs.

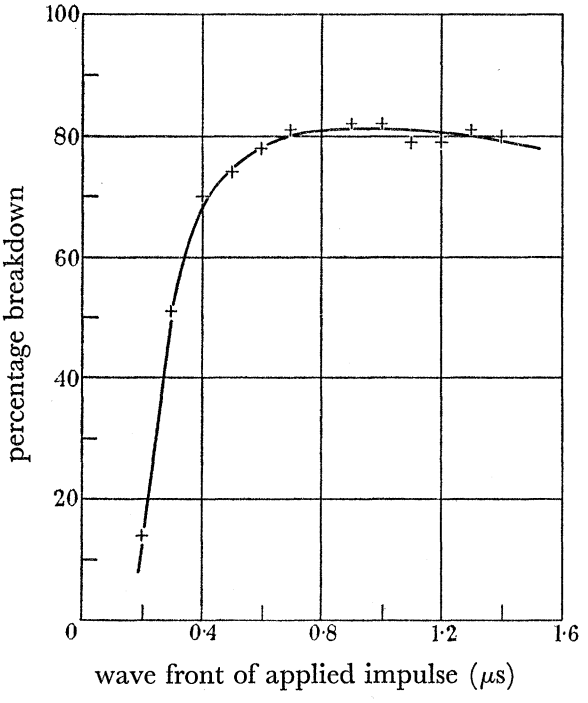

FIGURE 7. Effect of wave front on the breakdown probability of a 76·2 cm rod/rod gap for 490 kV crest voltage.

The breakdown voltage curves exhibit first a rise and then a fall with decreasing wave front, this maximum being especially well marked for 50% breakdown of short time lag.

The general characteristics of the histograms were:

(*a*) Few long time lags occurred at the fastest wave front, especially for the shorter gaps.

(*b*) Few long time lags occurred at the slower wave fronts, especially for the longer gaps.

An interesting effect was observed when rod electrodes of square section were used. Whereas observations normally show a decrease of mean time lag with increasing voltage, in this case the breakdowns of long time lag underwent a mean increase of 200 μs. This increase of the time lag was observed to occur between the voltage corresponding to 100% breakdown and the voltage mostly resulting in breakdowns of short time lag. However, the replacement of the earthed rod by a plane cathode eliminated the effect even for a square-section rod. Intense irradiation from the nearby impulse generator switching gaps was also found to destroy the effect, but not to remove the presence of long

PHILOSOPHICAL TRANSACTIONS OF THE ROYAL SOCIETY A MATHEMATICAL, PHYSICAL & ENGINEERING SCIENCES

time lags. Shielding experiments showed that irradiation of the anode region was the cause of this change.

The breakdown of a 76·2 cm rod/rod gap with impulses of wave front 0·50, 0·35 and 0·20 μs was examined with the streak camera. Figure 9 (*a*), plate 7, shows an arrested breakdown of short time lag obtained with the 0·50 μs wave front at 500 kV. Again two cathode discharges were observed, the second and greater discharge following after an interval varying between 0·6 and 1·9 μs. The second discharge was present in all cases of breakdown, but was often absent when sparkover failed to take place. The anode corona may again be of narrow structure, as shown in figure 9 (*b*), obtained at 475 kV.

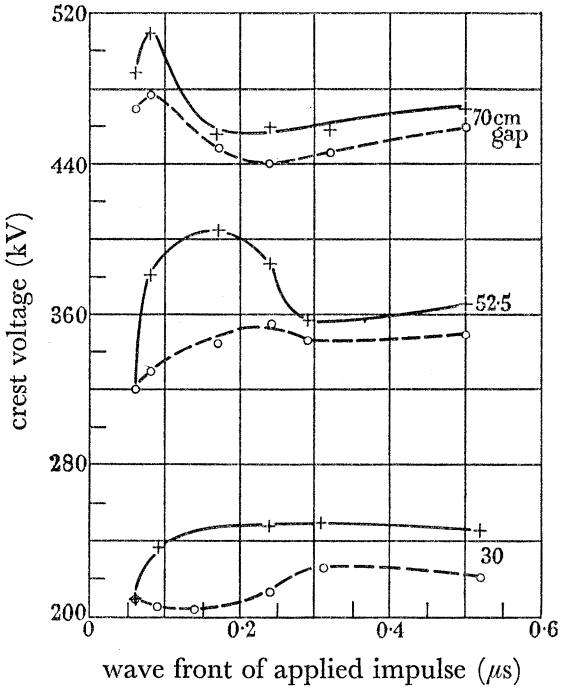

FIGURE 8. Variation of rod/rod gap breakdown voltage levels with impulse wave front. +, Points for 50 % breakdown after short time lag; ○, points for 50 % breakdown.

At 0·35 μs wave front the corona was usually of narrow structure; figure 9 (*c*) is an example of the two types.

Impulse-to-impulse variations in the corona structure were not apparent with impulses of 0·20 μs wave front. The corona channels up to a distance of 15 cm from the anode were of large radius, while beyond this were narrow channels. This is clearly visible in figure 9 (*d*), which is a breakdown of time lag 40 μs. The initial cathode discharge produced by this wave front was consistently smaller than that at 0·50 μs wave front. In the discharge of figure 9 (*d*) the second cathode discharge was particularly persistent, extending over a period of 5 μs; when sparkover began the positive leader again propagated well before the negative leader. Figure 9 (*e*) shows a breakdown of short time lag at 515 kV, with the second cathode discharge clearly visible. Once more, the anode leader precedes the formation of the cathode leader.

PHILOSOPHICAL TRANSACTIONS OF THE ROYAL SOCIETY A MATHEMATICAL, PHYSICAL & ENGINEERING SCIENCES

(*c*) *Rod/plane gaps*

The variation of breakdown voltage with electrode spacing of a hemispherically ended rod/earthed plane gap is shown in figure 10. These results differ from the behaviour of rod/rod gaps in two important respects:

(1) The breakdown voltage was less than that of the rod/rod gap by about 10% for the shorter gap spacings and 15% for the longer spacings.

(2) No change in the breakdown voltage was found for a reduction in the impulse wave front from 0·50 to 0·20 μs.

The breakdown voltage was well defined for all gap lengths, the transition range from 0 to 100% breakdown requiring merely a 6 to 8% increase in voltage. Also shown in the figure are the results of Allibone, Hawley & Perry (1934), whose data have been reduced by 4% to yield the 50% breakdown voltage, and those of Bellaschi & Teague (1934)and Gorev, Zalesky & Riabov (1948).

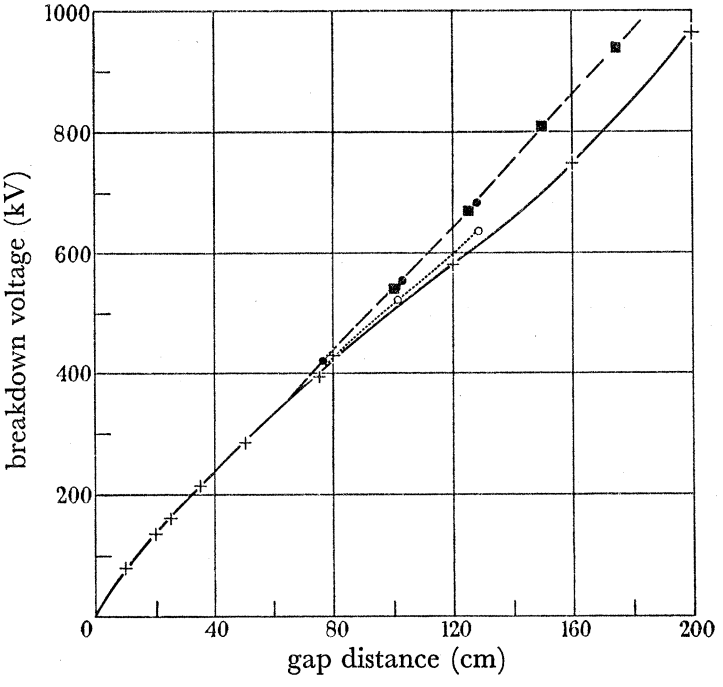

FIGURE 10. Breakdown voltages for rod/plane gaps. +, Present experiments, wave shape 0·20/2000 and 0·50/2000 μs; ○, ●, Allibone *et al.* (1934) 1/580 (○), 1/50 (●); ▪, Bellaschi & Teague (1934) 1·50/40 and Gorev *et al.* (1948) 1·50/40.

Time-lag measurements obtained in conjunction with the construction of figure 10 reveal that no long time-lag breakdown occur for gaps of 75 cm or more, a pattern similar to that found for the rod/rod gap. They became more common as the gap length was reduced, so that for a 10 cm gap at the 100% breakdown voltage, 60% of the breakdown were of this type. The mean short time lag varied with gap distance. For a 200 cm gap it was 22 μs, for 50 cm spacing 10 μs, and for 25 cm approximately 4 μs. This proportionality of time lag to gap spacing was found by Allibone *et al.* (1934).

Figure 10 shows good agreement between the present measurements and the data of Allibone *et al.* over the shorter gap lengths despite the difference in impulse wave tail and

the observed presence of long time lags. This results from the transition to breakdowns of short time lag for merely small overvoltages. The wave-tail sensitivity found by Allibone *et al.* for longer spacings was due to the appreciable formative time lag rather than the dead-time. No change in the distribution of time lags was brought about by change of the impulse wave front.

In contrast to the breakdown of rod/rod gaps, the discharge process in a rod/plane arrangement takes place entirely from the anode. Figure 11, plate 6, shows a discharge arrested a very short time before sparkover in a 2 m rod/plane gap at 950 kV; no leader grew from the plane electrode even at that late stage. The anode corona is seen to be composed of narrow channels, which were always observed at high crest voltages. The leader channel is accompanied by the glow discharge whose contour follows the lines of force between the leader and the plane.

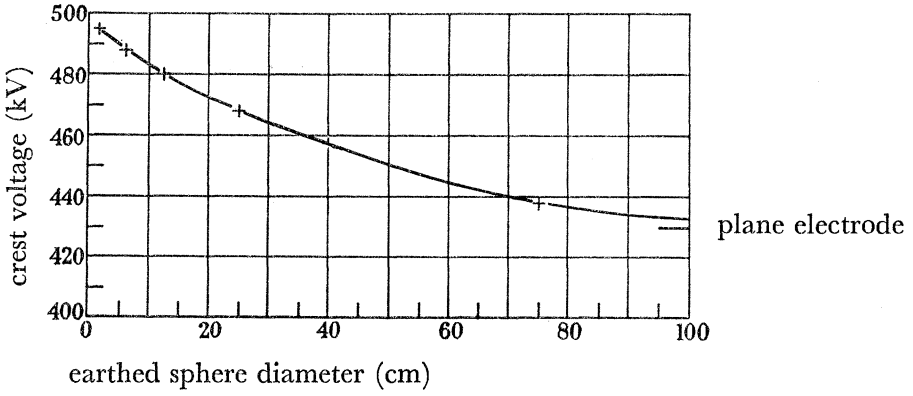

FIGURE 13. Variation of the breakdown voltage of a 80 cm rod/sphere gap with sphere diameter.

A rod/plane gap of 40 cm was also subjected to 0·50/2000 μs impulse potentials, at a crest voltage of 250 kV. Again no negative leader was observed up to the instant of voltage chopping. As in the rod/rod gap a dual character was found in the corona discharge at the high-tension anode. Figure 12 (*a*), plate 8, is a breakdown where the impulse corona shows a narrow channel structure, and figure 12 (*b*) reveals channels less numerous and of greater radius (both records were obtained with an image speed of 0·31 mm/μs). Of 52 records examined, 17 exhibited the narrow-channel corona and 35 the broader channels. Whereas all 17 of the former resulted in breakdown, only 15 cases of sparkover followed the broader channel corona discharges. The photographs obtained with no-breakdown impulses also proved of interest: on some occasions a series of small corona discharges of a mean frequency of 86 kc/s occurred in the anode region (figure 12 (*c*), image speed 0·069 mm/μs), while a much lower discharge frequency is seen in figure 12 (*d*) (0·069 mm/μs). These sometimes led to a sparkover of long time lag.

(*d*) *Rod/sphere gaps*

Because of the large difference between the breakdown voltage of the rod/rod and rod/plane gaps, measurements were made upon 80 cm gaps of intermediate geometry. A rod anode opposed by cathodes successively consisting of 6·25, 12·5, 25 and 75 cm diameter spheres was subjected to 0·50/2000 μs impulse potentials. The 50% breakdown

voltage is plotted in figure 13 as a function of cathode diameter. The rate of fall of breakdown voltage with increasing cathode diameter is greatest at small diameters; there appears to be no critical diameter indicating a change in the mode of breakdown despite the different growth observed between rod/rod and rod/plane discharges. The time-resolved photographs of figure 14, plate 9 (image speed 0·31 mm/μs), show that an upward-developing negative leader was initiated even when the cathode diameter was increased to 12·5 cm. For a 25 cm sphere, however, it was absent at least for the major part of the formative time.

(*e*) *Sphere/rod gaps*

When the high-tension rod electrode was replaced by a 75 cm diameter sphere opposing an earthed rod cathode, a large increase in breakdown voltage was observed. A crest voltage of 900 kV was required to ensure the breakdown of a 65 cm gap. Time-resolved photography (a typical record is that of figure 15, plate 9) showed that the initial breakdown took place in the form of a corona discharge from the rod electrode; this is not strongly recorded since the photograph was obtained with an $f/2{\cdot}5$ glass lens, in order to obtain a high image speed (1·2 mm/μs). The corona channels traversed the gap and initiated straight ionized paths from the anode. Precise time measurements showed that the positive and negative leader channels developed simultaneously. The high mean electric field in the gap resulted in a fast rate of discharge growth and consequently a short formative time lag (1·5 to 2·0 μs).

4. Discussion

(*a*) *Impulse breakdown voltages*

It is known from published data (Allibone 1937; A.I.E.E. Standard no. 4, 1940) that the breakdown of long inhomogeneous-field gaps is characterized by:

(1) High impulse ratios, 1·2 to 1·4 times the power-frequency breakdown voltage, the negative impulse ratio being higher than the positive impulse ratio.

(2) Ill-defined breakdown voltages, necessitating the definition of breakdown voltage as that resulting in breakdown of the gap upon 50% of impulses.

When impulses of sufficient duration are employed, it has been shown that the time lag of the breakdown may be short, governed only by the formative time, or long, due to the occurrence of a dead-time. The impulse wave-tail commonly used has a time to half-value of 50 μs. This is sufficiently long to allow the completion of all discharges of short time lag, but excludes those of long time lag. The existence of the transitional voltage range from 0 to 100% breakdown is therefore due to the increasing probability of short time-lag breakdown rather than decrease of the mean formative time lag or in the random scatter about this value.

(*b*) *Space charge modification of the applied electric field*

The existence of long time lags and the dead-time must be explained in terms of space-charge modification of the initial electric field by the impulse corona. It is therefore necessary to determine whether the charge observed to flow in the impulse corona is sufficient to cause appreciable modification of the initial electric field in the gap.

It has been established by Trichel (1938) and Loeb, Kip & Hudson (1941) that the corona current flowing from a sharp point maintained at a steady potential is discontinuous

in character, and that this discontinuity is due to the self-quenching of the discharge by its own space charge. The self-quenching of such discharges is aided by the extreme divergence of the electric field.

Impulse corona discharges from rod electrodes have been examined by Saxe & Meek (1955), Park & Cones (1956) and Brago & Stekolnikov (1958). The current wave form was found to consist of a fast rise (approximately 10^{-8} s) and a slower decay (approximately 10^{-7} s to half-value). The quantity of charge flowing in the impulse corona for a given gap voltage was found to vary with the gap distance. This is to be expected in the inverted rod/plane geometry that was used, since Park & Cones have shown that the gradient at the surface of the earthed rod depends critically upon the gap distance. For the high-tension rod/plane arrangement used in the present work this is not the case, except for short gaps.

Both Park & Cones, and Brago & Stekolnikov showed that the peak current of the corona discharge was directly proportional to the voltage at which the discharge occurred on the rising voltage wave front. The former also found an approximately linear relation between the peak current and the extent of the corona channels.

These results suggest that the total charge conveyed into the discharge space is roughly proportional to the square of the applied voltage, and that the extent of the corona channels varies linearly with voltage. This was found in the present work.

The constant corona channel velocity during growth encourages an assumption of uniform characteristics along their length. If it is assumed that the net space charge indicated by the corona current is distributed as a constant charge/unit length along the channels, the gradients set up by this space charge can be estimated. Since the number of channels is large, the corona discharge can be approximated by a hemispherical cloud, the charge density of which is inversely proportional to the square of the distance from the electrode. (Park & Cones suggested a space charge density inversely proportional to the distance from the electrode. It is difficult to reconcile this distribution with the assumption of uniform conditions along the length of the corona channels.) Then in Appendix II it is shown that the axial space charge field at a distance $(s-r)$ metres from the surface of the high-tension rod is given by

$$E_s = \frac{300Q}{Rs^2}\left[r\ln\left\{\left(R^2+\frac{r^4}{s^2}\right)^{\frac{1}{2}}-\frac{r^2}{s}\right\}\right.$$
$$\left.-r\ln\left\{\frac{r}{s}(r^2+s^2)^{\frac{1}{2}}-\frac{r^2}{s}\right\}+R+r-2s-(R^2+s^2)^{\frac{1}{2}}+(r^2+s^2)^{\frac{1}{2}}\right]\text{V/cm}, \qquad (1)$$

where Q e.s.u. = net charge on corona channels,

R cm = radius of corona hemisphere,

r cm = radius of spherical electrode tip.

The form of this field is plotted in figure 16 for an observed corona discharge at 950 kV impulse crest.

The net field prevailing at any point in the gap as a result of space charge formation is the sum of the field E_s given in equation (1) and the gradient $\bar{E}_s$ resulting from the applied potential difference across the gap. By means of a resistor network analogue it was found

that the potential at S, a distance s metres along the gap axis from the electrode spherical tip centre small compared with the gap length, is described well by the empirical formula

$$V_s = V_r\left(\frac{r}{s}\right)^{\frac{1}{2}}, \tag{2}$$

where V_r is the potential of the electrode.

The gradient $\bar{E}_s$ at S is thus

$$\bar{E}_s = -\frac{V_r}{2}\left(\frac{r}{s^3}\right)^{\frac{1}{2}} \text{ V/cm}. \tag{3}$$

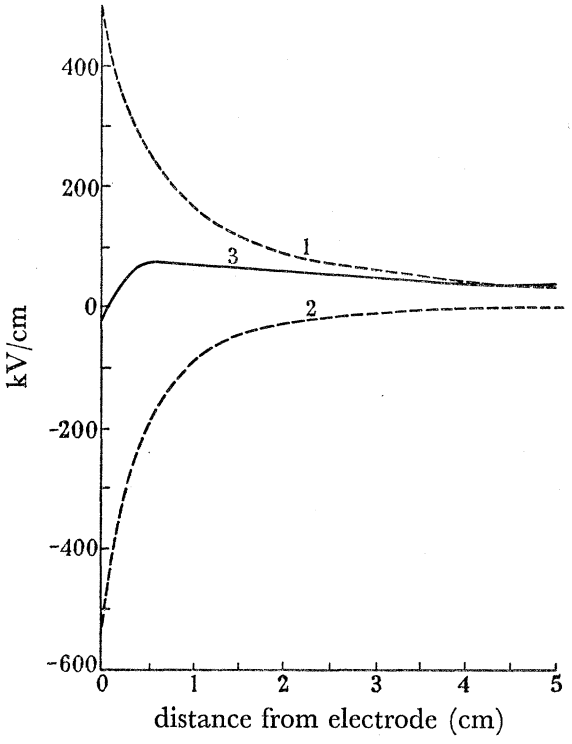

FIGURE 16. Space charge modification of the electric field near a rod electrode. Curve 1, applied field; 2, space charge field; 3, net field.

$\bar{E}_s$ is shown as a function of $(s-r)$ in figure 16, again for the case $V_r = 9{\cdot}50 \times 10^5$ V and $r = 0{\cdot}95$ cm. The net field $E_s + \bar{E}_s$ is also plotted. It is seen that the maximum gradient in the gap is reduced from 530 kV/cm to about 75 kV/cm as a result of the 11·5 μC charge flow taking place in the corona stage of the discharge. The expression inside the square brackets of equation (1) is not sensitive to change of R except at small R. Thus, since Q/R varies linearly with V_r, similar field reductions to that in figure 16 have been found for observed impulse corona growths at other electrode potentials.

Park & Cones found that a distribution of space charge of density inversely proportional to the square of the distance from the electrode would give a higher electric gradient than that prevailing in the absence of space charge. The reason for this is that the electrode geometry was represented by a pair of concentric spheres. This would yield a more highly divergent initial electric gradient than has been shown in equation (3); a space charge density decreasing linearly with increasing distance from the centre of the system would then yield uniform electric gradient.

(*c*) *The statistical time lag*

In considering the criteria for the initiation of long-gap breakdown, the distinction between the corona and leader channels is of prime importance. The corona channels propagate at velocities of the order of 10^8 cm/s, but are of low ion density and do not constitute an effective breakdown of the gap. The slower leader channels, on the other hand, involve approximately 0·01 % ionization of the gas.

The breakdown level of an inhomogeneous-field gap is determined by the conditions required for the establishment of a highly ionized leader stage, these conditions then being easily adequate for the successful completion of the discharge. The existence of dead-times shows that the disposition of the electric field and/or the supply of electrons for the initiation of ionization may be more favourable for the propagation of the leader channel at some time on the wave tail rather than immediately the potential difference is applied across the gap. The probable cause of breakdown will, however, be governed by the nature of the corona burst. It is necessary to consider the causes of variation in this initial partial breakdown of the gap.

Although the mean corona space charge content increases with increasing crest voltage for a given wave front, there are considerable pulse-to-pulse variations. Because of the important influence of this space charge upon the electric field in the gap, this random behaviour must largely account for the statistical nature of long gap breakdown. Variability in the time of appearance of the primary electrons, i.e. the statistical time lag, must be the main cause of these fluctuations. Variations in the impulse wave front would aggravate these fluctuations, but no such variations could be detected in the experiments.

It is clear that the discharge initiation cannot depend upon the production of ion pairs by natural radiations during the application of the impulse voltage. Any explanation of the effects observed at rapid wave fronts would require a far higher rate of electron appearance than is found to occur. Kuffel (1959) measured an indoor rate of production of only 20 ion pairs $cm^{-3}\,s^{-1}$.

Since the lifetime of a thermal electron in air is merely $\sim 10^{-7}$ s, owing to the affinity of oxygen for the attachment process, the most probable source of free electrons is from negative ion detachment. Loeb (1935) has shown that the O_2^- ion releases its electron at $E/p = 90$ V cm^{-1} $mmHg^{-1}$, the O ion being considerably more stable. The gradients in the inhomogeneous field near a rod are easily adequate to initiate this process. It has been found in the present experiments that $E/p = 60$ near the anode surface is sufficient to initiate the impulse corona shortly after the application of the impulse wave. No explanation can yet be given for this apparent increase in the probability of the detachment process. Nevertheless the importance of the detachment process also explains why the space charge distortion by the corona phase is so effective in preventing ionization during the dead-time. It is a less rigorous requirement to reduce the electric field so that no detachment occurs than to reduce the ionization coefficient α to very low values.

Mobility measurements upon atmospheric ions have shown that the size range is large. The smallest ions have a mobility of ~ 1 cm $s^{-1}(V/cm)^{-1}$ and a population of $\sim 300/cm^3$ (Chalmers 1957). The high mobility suggests that these are simple ions and thus it is probable that the population of the oxygen ions is of this order.

This density of ions suggests that it is probable that more than one electron will become available by detachment before the corona space-charge field seriously reduces the gradient near the anode. This is borne out by the increasing number, with increasing voltage, of corona channels initiated by highly ionized stems at the anode surface.

In discussing his experiments Loeb (1939) suggested that the O_2^- ion attained the energy for detachment in two free paths. Recently Muschlitz (1959) found a cross-section of 40 Å^2 for 6 eV O_2^- ions in oxygen, when detachment was an important process. This gives a mean free path of 7×10^{-3} cm. In the prevailing field the ion drift velocity is $\sim 10^5$ cm/s, thus the mean time to detachment would be $\sim 0{\cdot}15$ μs. This is not negligible with the wavefronts employed here. It is improbable, therefore, that the mean time required for detachment would change very rapidly with the rate of voltage application. This is shown by the results of Brago & Stekolnikov (1958) who measured the time interval occurring on an impulse wavefront between the time of attainment of the minimum corona ignition voltage and the mean time of appearance of the corona. Although the time interval decreased with increasing crest voltage, it tended to a minimum value of $\sim 0{\cdot}25$ μs.

The number of free electrons becoming available in the anode region depends upon the statistical variation of the mean detachment time lag and on the random disposition of negative ions in the high-tension region at the instant of impulse voltage generation. A further important variable is the rate of rise of the applied voltage, since the negative ion density in the vicinity of the anode will increase slightly during the statistical time lag owing to drift towards the electrode. The impulse wave front is also important in that, because of the appreciable detachment time lag, the gradient at which the free electrons appear will depend on the rate of voltage rise following attainment of the corona ignition voltage.

(*d*) *Impulse corona at the anode*

Since the number and timing of the initiating electrons will have an important effect on the corona discharge, which in turn will govern whether sparkover of the gap is probable, it is necessary to account for the positive corona variations in terms of the statistical time lag.

At voltages near the onset level no differences were observed either in structure or extent between the corona produced with 0·20 and 0·50 μs wave-front impulses. This is because the initiating electrons become available after the crest has been attained. At higher voltages it was found that the radius of the corona discharge was some 15% greater for the 0·20 μs wave front. This is due to the initiation of the impulse corona before the peak value of the applied voltage has been attained. The space charge being created by the corona opposes the applied field and thus has a self-quenching effect. Since the corona channels develop at a velocity of 10^8 cm/s, only a rapidly rising potential at the anode could maintain the propagation of the corona and so increase the radius of the discharge envelope.

Upon increasing the crest voltage it was found that the extent of the thicker corona channels was decreased and the corona envelope consisted mainly of numerous narrow channels. Then an extension of the preceding argument accounts for this change: in this case it is probable that the high rate of increase of gradient in the gap due to a steep wave

PHILOSOPHICAL TRANSACTIONS OF THE ROYAL SOCIETY A MATHEMATICAL, PHYSICAL & ENGINEERING SCIENCES

front and high crest voltage enables a sufficient potential gradient to be established to give more widespread detachments in the gas, despite the quenching effect of the already propagating broader corona channels. This explanation is supported by the observation that irradiation of the anode region encourages the onset of the narrow-channel corona at lower voltages, which suggests that these occur at higher free electron densities.

At higher voltages the narrow-channel corona becomes frequent even with 0·50 μs wave front. In this case no thick corona channels are present when the narrow channels occur. This difference from the 0·20 μs wave-front impulse may be due to the negative ion drift effect previously mentioned. A higher density of initiatory electrons will be available at the anode than for the faster wave front.

The pronounced increase in the corona along the length of the rod in cases where the narrow-channel corona occurs is also an indication of the initiation of the corona burst at a higher voltage level. The presence of the large diameter corona envelope reduces the potential gradient near the cylindrical rod surface, so that a gradient sufficient for negative ion detachment may never be attained if the corona burst is formed relatively early upon the wave front.

(*e*) *Rod/plane breakdown*

The empirical equation (3) shows that the applied field near a high-tension rod in a long gap is dependent only upon the geometry and potential of this electrode, and not upon the gap distance or geometry of the earthed electrode. Figure 17 is a graph of the variation of the axial electric gradient with distance from the high-tension electrode for various gaps, assigning unit potential to the rod, and assuming that surrounding walls, floor and ceiling are 3 m from the rod. Even where the gap is 15·2 cm (6 in.) the variation with gradient follows closely the curve for a 106·7 cm (42 in.) gap for some half of the gap. As would be expected, the effect of surrounding earthed surfaces makes the electric field in the vicinity of the earthed electrode, when this is of rod form, sensitive to gap spacing. Yet despite the independence of the field in the vicinity of the anode from gap spacing and cathode geometry, the leader channel is unable to become fully established in the absence of the earthed electrode. Thus no explanation of spark mechanism can be sought solely in terms of processes near the high-tension electrode, even though the applied electric field in this region can be up to two orders of magnitude greater than that at the earthed electrode.

The earthed cathode thus plays a vital role in promoting the breakdown of a long gap. Two possible mechanisms can be dismissed. First, in long gaps, so far as revealed by the *f*/1 camera, the corona produced at the rod anode by no means bridges the gap. (The Lichtenberg figures of Allibone (1938, 1948) and Baatz & Fischer (1961) show that the gap is bridged by the corona discharges. However, except for short gaps, the *f*/1 streak camera reveals that the corona discharges from the anode and cathode electrodes are not always synchronous and following the initial cathode discharge larger discharges may occur. In long rod/plane gaps where the anode corona is observed to bridge the gap (Allibone 1938), the initial electric gradient is higher than in the present experiments because of the increased voltage required to cause breakdown due to the use of a large series resistor.) Thus there is little possibility of secondary electrons becoming available from the cathode by positive ion or photon bombardment, or of local high fields being set up at the cathode

in the region of the partially conducting positive corona channels. In any event, the transit times in these gaps would be so long that the growth of ionization must be regarded as proceeding independently at both cathode and anode.

Secondly, it has been shown that for a cathode diameter exceeding 12·5 cm no discharge was observed at the cathode surface which would lead to any distortion of the field in favour of the anode region.

The remaining possibility arises from the effect of a plane cathode on the potential gradient in the gap as a result of the initiation of breakdown at the rod. The space charge

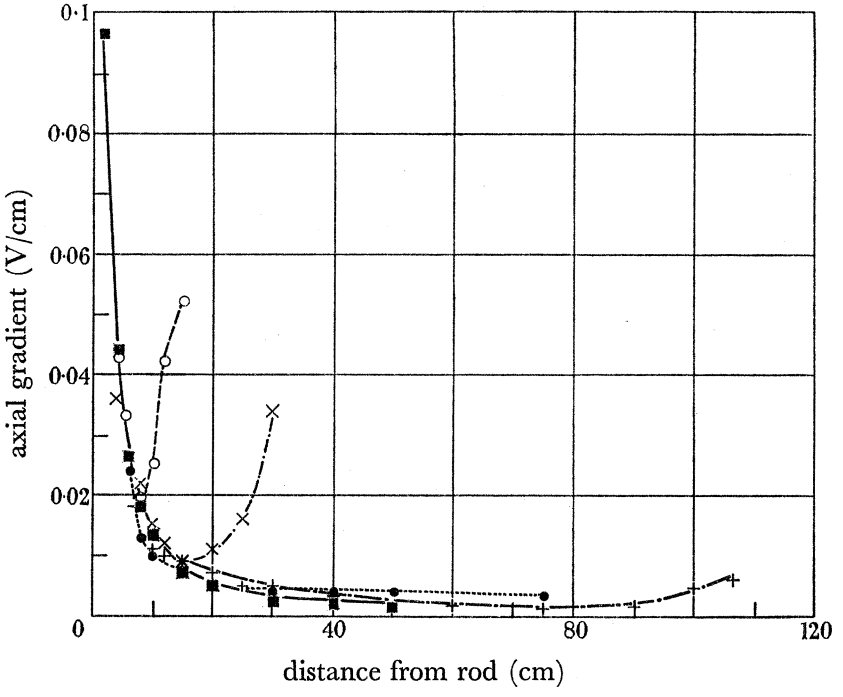

FIGURE 17. The axial electric gradient in long gaps for unit potential difference. Rod/rod gaps (cm): ○, 15·2; ×, 30·4; +, 106·7; rod/plane gap (cm): 76·2; ▪, calculated from equation (3).

Q created by the positive impulse corona induces a charge upon the plane which is electrostatically equivalent to an image charge Q' of equal magnitude (but opposite polarity) equidistant with Q behind the plane. The potential gradient produced by Q' at a distance d above the plane can be obtained from equation (1) by putting $Q' = -Q$ and $s = l+d$, where l is the gap spacing. In this way it is easily shown that, in the case of a 2 m rod/plane gap (the example used earlier), the gradient produced at the plane cathode surface is 635 V/cm; unlike the gradient produced at rod cathode, this is negligible.

However, the image charge Q' will produce a second image Q'' in the high-tension rod anode. Q'' will be of the same polarity as the actual space charge Q and will reduce its field-quenching effect. The results already quoted for the corona discharge in rod/plane gaps show that $R \sim \frac{2}{3}l$, for a wide range of l. Q' is therefore approximately $2R$ distant from the high-tension electrode, and the image charge produced in that electrode is $Q'' = -rQ'/2R = rQ/2R$. This will be positioned at a radius from the centre of the hemispherical termination of the rod of $r^2/2R$, i.e. very near the centre. The potential gradient

produced by Q'' at the anode rod surface is then very nearly $Q/2Rr$, and acts so as to augment the applied field. Again using the data for a 2 m rod/plane gap, the gradient produced in this way at the anode surface is found to exceed 40 kV/cm, falling off as the square of the distance from the rod centre of curvature. Since Q is proportional to the square of the impulse voltage and R varies linearly with voltage, the effect is directly proportional to voltage, and so reduces the space charge field by a constant factor. The effect may well be important in facilitating the propagation of the positive leader in rod/plane breakdown, but will diminish at an increasing rate as the radius of the cathode is decreased. The probability of breakdown of rod/sphere gaps exhibits such a decrease. The effect would be negligible in a symmetrical rod/rod gap, for example, since $Q'' \sim Qr^2/l(l-R)$, a very small value.

(f) *Rod/rod breakdown*

(i) *General considerations*

When the cathode is of small dimensions its contribution to the breakdown process will be of a different nature. Here the field at the earthed rod will increase appreciably by virtue of the space charge formed in the anode region. An approximate calculation indicates that this increase will be tenfold, and is sufficient for ionization to occur at the cathode. The corona discharge which is so initiated results in a negative space charge surrounding the cathode, reducing the field at the cathode surface but increasing the mid-gap field ahead of the immature leader channel formed at the anode (Waters & Jones 1961). Such an increase, although small, may well be critical in aiding the propagation of the leader channel through the region occupied by the anode corona, since the field is here lowered by the positive space charge. Again, the displacement current due to the negative corona discharge which will flow in the positive leader will cause further ionization tending to lower its resistivity and so increase the electric gradient at its head (Waters 1962).

Such a model seems to provide the only means of accounting for the increase of breakdown voltage of a rod/rod gap with increasing gap length. The amount of space charge necessary to initiate ionization at the earthed electrode will increase approximately as the square of the gap length. Since the charge content of the high-tension corona increases as the square of the applied voltage there will be an approximately linear relation between the breakdown voltage and gap length for all gap lengths. This is found to be the case.

The contribution to the growth of the negative leader channel which is observed to form in rod/rod and other gaps in which the radius of curvature of the cathode is not too large also requires consideration. The onset of the negative leader might, for example, be thought to be the criterion for breakdown in such gaps. The evidence does not support this conclusion. For example, figure 13 showed no discontinuity or sudden increase in breakdown voltage for those gap configurations for which no negative leader is observed. On the contrary, the critical level decreased as the axial electric field became more asymmetrical in favour of the anode region. Again, the photographic records for all gap arrangements (including spherical anode/earthed rod, in which the anode field is low and the cathode field high) show that the negative leader does not precede the positive leader in time. The lower the field at the cathode, the later is the appearance of the negative leader channel relative to that of the positive leader. It seems clear that the initiation of the negative leader is a consequence of the induced field at the cathode surface due to the

approach of the positive leader. The latter will have already developed a sufficiently high ion density to have reached a self-propagating condition, although the approach of an oncoming leader of opposite polarity will aid its growth.

(ii) *Breakdowns after long time lags*

The leader channel represents the extension into the gap of one or more highly ionized stems produced during the corona phase near the anode surface (Brago & Stekolnikov 1958). In cases where breakdown successfully results from the uninterrupted propagation of this channel across the gap, the breakdown is of normal short time lag. When the anode leader is not formed at this stage, the prevailing electric field will subsequently be too low for any further ionization activity. There will then be a dead-time during which no ionization occurs, as recorded by time-resolved photographs. The length of the dead-time depends on the recovery of electric gradient due to the movement of space charge. This space charge consists of positive and negative ions of mobility about 1 cm s^{-1} $(V/cm)^{-1}$. Since the maximum field in the gap is about 70 kV/cm, the observed dead-times of the order of 100 μs are sufficient to permit appreciable space charge movement.

The time-lag histograms show that long time lags are absent for positive impulses in the longer gaps except for fast wave fronts (or, more accurately, the dead-time is so long relative to the impulse wave tail that no breakdown takes place).

During the space-charge drift the electric field will increase at both electrodes—at the high-tension electrode owing to space-charge removal, and at the earthed electrode owing to its approach. At the breakdown voltages of shorter gaps, the corona space charge may be sufficiently small for its effect to be diminished appreciably during the impulse duration by the drift process. At the higher voltages required for long gaps the corona space charge may not be cleared from the anode region sufficiently quickly. The space charge drift, however, could cause a corona discharge to occur from the cathode surface (as, for example, in figure 9 (*d*)), provided that the high-tension corona space charge was sufficiently great. This would be the case for fast wave-front impulses. Such a cathode discharge would then lead to an increase in the potential gradient in the anode region and increase the probability of positive leader formation. This suggestion is fortified by the absence of long time lags in long rod/plane gaps, even for fast wave-front impulses, where the cathode field is too low for a discharge to occur.

(iii) *Corona at earthed cathode*

The leader from the earthed cathode initiates relatively later in the development of the positive leader the greater the gap distance and the greater the radius of the cathode.

The corona discharge at the cathode, on the other hand, occurs after little delay, and plays an important part in determining the progress of the discharge in the anode region. The main experimental observations on the cathode discharge are summarized in Appendix I.

The streak photographs show that the anode corona in gaps of length 40 and 55 cm often show a narrow structure which is not observed at those voltages when the opposing earthed rod or plane is removed. This is also true to a lesser degree for a 76·2 cm gap. For the rod/rod gap this change of structure must be brought about by the initial cathode

corona discharge, since, unlike the rod/plane configuration, the space charge field would be little modified by the presence of the earthed rod itself.

It is probable, therefore, that a typical breakdown sequence of a rod/rod gap proceeds as follows:

(1) The onset of ionization following the statistical time lag initiates the anode corona discharge.

(2) The immediate increase in potential gradient at the cathode caused by anode space charge produces the initial corona discharge at the cathode.

(3) The cathode discharge acts reciprocally upon the anode gradient to increase the space-charge content of the positive corona. When the cathode discharge is large, the field increase may be sufficient to bring about detachment and the formation of narrow anode corona channels.

(4) The positive leader is formed at this early stage as a result of heavy ionization near the anode surface.

(5) The space charge is distributed throughout the positive corona. This equilibrium will not be attained immediately owing to the limited conductivity of the corona channels. This increases the field at the cathode, and a further discharge occurs at this electrode. The greater intensity of this secondary discharge may be due to the ionization produced during the first cathode discharge.

(6) Again the anode field is intensified as a result of the cathode discharge, and the immature positive leader is helped to propagate.

The gap size and applied impulse wave shape will influence this pattern to a considerable degree. For short gaps the discharge from the earthed rod is so extensive that the consequent space charge prevents the occurrence of any further cathode discharge; when breakdown occurs the negative leader is initiated rapidly.

In long gaps, on the other hand, the influence of the initial cathode discharge upon the development of the positive corona will be negligible; the probability of breakdown will depend upon the ability of the positive corona space charge to initiate a second cathode discharge.

(iv) *Influence of wave front on breakdown probability*

The amount of ionization taking place in the anode corona is of importance in determining the successful establishment of the leader channel both by its provision of adequate initiation conditions and its influence in determining the aid given by the cathode discharge. Since it has been shown experimentally that the impulse wave-front duration influences both the anode corona and the probability of breakdown of the rod/rod gap, it remains to explain the latter correlation in terms of the former. It is also pertinent to comment here that, since in the rod/plane discharge no cathode corona occurs, there is no variability of breakdown probability with wave front.

Short rod/rod gaps (<40 cm). At low voltages the positive corona consists of broad channels. An increase of the rate of rise of the impulse potential does not affect the structure but increases the length of the channels and the amount of space charge injected into the gap. The breakdown voltage would thus be expected to vary little with wave front, except to exhibit a fall at fast wave fronts. This is observed (figure 8). At the

breakdown voltage of short gaps the space charge content of the anode corona is small. In addition the mid-gap field in short gaps is fairly high and enables the space charge clearance time to be within the impulse duration; thus breakdowns after long time lags are observed for all wave fronts except the fastest of 0·06 μs. The unusual increase of time lag with increasing voltage for these delayed breakdowns implies that the greater quenching space charge outweighs the faster drift in the applied field.

Intermediate rod/rod gaps (40 to 70 cm). At the impulse crest voltages associated with the breakdown of gaps in this range, the anode corona structure is more variable. With a 0·50 μs wave front some impulses yield narrow corona channels; this type of corona has been shown to lead to a higher probability of breakdown than the broader corona, probably due to a slightly higher space charge content. Its occurrence at lower voltages in the presence of the earthed electrode has already been ascribed to the influence of the first corona discharge. At higher voltages the prevalence of the dual corona structure may account for instabilities in breakdown voltage associated with a 55 cm gap.

For an impulse wave front of 0·20 μs the breakdown probability is reduced; associated with this is the onset of long time-lag breakdown. This suggests a lower space charge content than that produced by the 0·50 μs wave front. Now in this case no variation of the corona form is found from pulse to pulse; as in the case of an isolated anode under 0·20 μs wave fronts and medium voltages, it consists of an inner region of broad channels and an outer region of narrow channels. The first cathode discharge is weak and appears not to modify the high-tension corona form. The difference in breakdown probability between the 0·20 μs and the 0·50 μs wave fronts must be sought in terms of the current associated with the anode corona. This appears greater at 0·50 μs wave front so as to cause a more vigorous cathode discharge. This may be explained by considering again the effect of ion drift during the wave front; the time taken for the applied field to attain the corona ignition level is longer for slowly rising waves, thus the number of initiating electrons will be greater.

For very fast wave fronts the voltage at which the corona ignites is high, since the statistical time lag does not decrease rapidly with overvoltage. The heavy ionization which is caused compensates for the reduction in the number of initiatory electrons. The consequent increase in magnitude of the anode corona will then lead to the decrease in breakdown voltage and absence of long time-lag breakdown which is observed.

Long rod/rod gaps ($>$70 cm). Since for longer gaps the first cathode discharge will have little influence upon the high-tension corona, the breakdown probability depends solely upon the numbers of initiating electrons and the point upon the wave front at which they become available. With decreasing wave front a fall is at first observed in the breakdown voltage characteristic. This is accountable in terms of the increase in the level at which the corona is ignited. The increased breakdown voltage for faster wave fronts must again be ascribed to the decreasing number of ions available for detachment when igniting potential is quickly reached.

For nearly square waves the breakdown voltage again decreases owing to the extremely high corona onset potential.

5. Conclusions

(*a*) The impulse corona phase injects sufficient space charge into the region surrounding the high-tension anode in rod/rod or rod/plane gaps to modify seriously the applied field.

(*b*) The statistical nature of the breakdown results from random variations in the impulse corona; this in turn is due to variability of the number and the time of appearance of the initiatory electrons.

(*c*) The electron supply is probably from negative ion detachment. The efficiency of space charge quenching is the result of the prevention of detachment.

(*d*) The earthed electrode plays an essential part in the initiation of the leader stroke, even though its influence on the applied electrostatic field near the anode is small.

(*e*) The negative leader is initiated as a result of the formation of the positive leader. The influence of cathodes of small dimensions upon the growth of the discharge is due to the corona burst caused at its surface. For large cathodes a reduction of the space charge quenching of the anode electric field is brought about due to induced charge on the cathode surface, which in turn augments the anode gradient.

(*f*) The effect of wave front upon breakdown voltages can be interpreted in terms of the changing character of the positive corona with rate of potential rise at the anode.

(*g*) The transitional character of the impulse breakdown level of long gaps is due to the existence of long time lags.

(*h*) Breakdown after long time lags, and high impulse ratios, are due to the space-charge field modification.

(*i*) Reproducibility of breakdown voltages in different laboratories can be expected only if the wave front of the applied impulse, the gap geometry and the atmospheric conditions (including, possibly, the concentration of ions) are closely specified.

The authors wish to express their gratitude to Dr T. E. Allibone, C.B.E., F.R.S., Director of the Laboratory, who initiated this research, for his continued interest, help and valuable advice and for permission to publish these papers to Mr D. P. R. Petrie for useful discussion and encouragement; to Dr G. D. Archard for his work with the resistor network analogue; and to Mr C. J. Bulcock for aid with the experimental work.

Appendix I

(*a*) *Anode corona discharge*

Discharges occurring with impulses of various crest voltages were photographed with the *f*/1·0 camera. In order to eliminate cathode effects the nearest object to the rod was the laboratory floor, at a distance of 300 cm. Two wave fronts of 0·20 and 0·50 μs duration respectively were applied in turn to the rod. A corona discharge was observed for 50% of the impulses when the crest voltage reached 90 kV. Since at this minimum voltage the onset of corona discharge was found to be delayed by as much as 10 μs following the commencement of potential rise, no differences in the onset potential or in the corona structure were found for the two different wave fronts. In both cases the length of the corona discharge was 4 cm, consisting of an average of three channels of radius approximately 0·1 cm.

At higher voltages the delay in initiation became shorter and when the corona occurred on the potential wave front differences became observable; the corona envelope was 15% more extensive for the faster wave front (figure 1 (*a*) and (*b*)). Both corona discharges consisted of channels of radius up to 0·3 cm. With further increase in voltage a striking

change in the form of the corona produced by the 0·20 μs wave-front impulse occurred. The discharge then no longer consisted solely of broad channels, but also contained many more channels of narrow structure; the extent of the broader channels was reduced. The estimated radius of the narrow channels was 0·02 cm. This transition was not complete, both types of corona discharge occurring over a voltage range of 150 kV. These are illustrated in figure 1 (*c*) and (*d*). The voltage producing an equal proportion of the narrow channel corona and the broader channel corona was found to be subject to short-term variation, and was unlikely to be reproducible from day to day. The mean voltage was 350 kV. This was also true for the 0·50 μs wave-front impulse, where the transition occurred at a higher crest voltage of 550 kV. In this case, however, the broad channels disappeared completely in corona where the narrow channels were observed. At both the wave fronts employed it was noticeable that, when the corona discharge consisted of the narrow channels, considerably more extensive corona discharge also occurred along the length of the rod (figure 1 (*c*)).

The crest voltage at which the transition from broad to narrow corona channels took place could be reduced by half for each wave front when radiation was present from a 1 mc Co 60 source placed within the hollow anode.

Further increase in the crest voltage of both wave shapes resulted merely in increasing the extent of the corona channels without further changes in appearance.

(*b*) *Cathode corona discharge in rod/rod gaps*

The time-resolved photographs of rod/rod breakdown showed the following variations in the corona discharge at the earthed electrode:

(1) The intensity of the impulse corona discharge decreased with increasing gap spacing.

(2) For a given gap spacing the intensity of the cathode corona increased with increasing wave-front duration.

(3) At gap spacings where, from pulse to pulse, high-tension corona of both narrow and broad structure were found, the finer anode corona is accompanied by the more energetic cathode corona discharge.

(4) For the longer gaps the weak first discharge was followed by a stronger second discharge, or several discharges. The delay between the first and second cathode discharges increased with increasing gap spacing and, for a given gap spacing, with decreasing voltage.

(5) The secondary cathode discharge accompanies a stronger propagation of the anode leader. In the majority of photographs of impulses failing to bring about breakdown, the secondary discharge is absent.

Appendix II. Corona space-charge field calculation

The amount of charge in a hemispherical shell of thickness dx at any radius in the corona cloud defined in §4 (*b*) will be $A\,\mathrm{d}x$, where A is a constant. The charge density ρ_x at a distance x cm from the electrode centre is thus

$$\rho_x = \frac{A}{2\pi x^2} = \frac{Q}{2\pi R x^2}. \qquad (4)$$

Suppose *APB* (figure 18 (*a*)) represents the hemispherical electrode tip. For the purpose of calculating the axial gradient the error will be small (Park & Cones 1956) if the image charge is assumed similar to that produced in a spherical conductor. Then an element of space charge at radius x will have an image in the electrode at radius $y = r^2/x$. This image charge is $-r/x$ times the actual charge.

Thus the charge on a hemispherical space charge shell of radius x is

$$q_x = \rho_x 2\pi x^2 \, \mathrm{d}x \tag{5}$$

and that on the corresponding image element is

$$q_y = -\rho_x 2\pi r x \, \mathrm{d}x; \tag{6}$$

therefore

$$\rho_y = -\frac{x^5}{r^5}\rho_x. \tag{7}$$

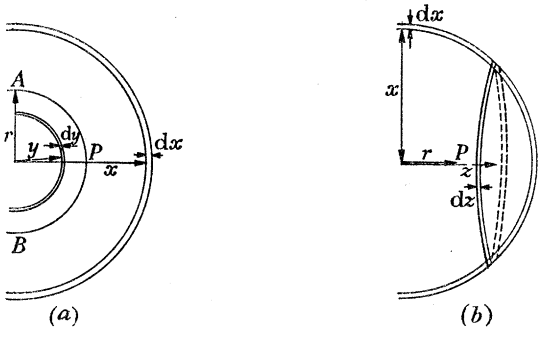

FIGURE 18. (*a*) Cross-section of sphere charge shell, hemispherical electrode and image charge shell. (*b*) Subelements of space charge shell.

Then the charge/unit area on the space-charge element is $\rho_x \mathrm{d}x$, and on the image element

$$\rho_y \, \mathrm{d}y = \frac{x^3}{r^3}\rho_x \, \mathrm{d}x. \tag{8}$$

The potential at P due to an element of space charge at x may be found by considering subelements of thickness $\mathrm{d}z$ (figure 18 (*b*)):

$$V'_P = 300 \int_{z=0}^{x} \frac{2\pi x \, \rho_x \, \mathrm{d}x \, \mathrm{d}z}{[(z-r)^2 + (x^2 - z^2)]^{\frac{1}{2}}}$$

$$= \frac{600\pi\rho_x x \, \mathrm{d}x}{r} [(r^2 + x^2)^{\frac{1}{2}} + r - x] \text{ volts}. \tag{9}$$

Similarly, it can be shown that the potential at P due to the corresponding element of image charge is

$$V''_P = -V'_P. \tag{10}$$

Thus the potential at P is zero, as required.

The electric field at P is found by differentiating V'_P and V''_P with respect to r. The field due to the space-charge element is

$$E'_P = \frac{600\pi\rho_x x \, \mathrm{d}x}{r^2} \left[x - \frac{x^2}{(r^2 + x^2)^{\frac{1}{2}}} \right] \text{volts/cm}, \tag{11}$$

and that due to the image charge element is

$$E''_P = \frac{600\pi\rho_y\, y\, dy}{r^2}\left[y+\frac{y^2}{(y^2+r^2)^{\frac{1}{2}}}\right]$$
$$= \frac{600\pi\rho_x\, x\, dx}{r^2}\left[r+\frac{r^2}{(r^2+x^2)^{\frac{1}{2}}}\right] \text{volts/cm.} \qquad (12)$$

The total field at P due to the hemispherical space charge and its image is

$$E_P = \int_r^R (E'_P+E''_P)$$
$$= \frac{300Q}{Rr^2}\left[R-(R^2+r^2)^{\frac{1}{2}}+r(\sqrt{(2)}-1)+r\ln\frac{(R^2+r^2)^{\frac{1}{2}}-r}{(\sqrt{(2)}-1)\,r}\right] \text{volts/cm.} \qquad (13)$$

At a point S, distant $(s-r)$ from the electrode surface, the gradient due to the image charge is

$$E_{s1} = \int_r^R \frac{300Q}{Rs^2}\left[\frac{r}{x}+\frac{r^3/s}{x\left(x^2+\frac{r^4}{s^2}\right)^{\frac{1}{2}}}\right]dx. \qquad (14)$$

The gradient due to the actual space charge is of two opposing parts: first, a gradient E_{s2}, opposing the applied field, due to the space charge in the spherical cap between $s \leqslant x \leqslant R$, and secondly a gradient E_{s3} due to the remaining space charge. The net field will thus be

$$E_{s3}-E_{s2} = \int_s^R \frac{300Q}{Rs^2}\left[1-\frac{x}{(x^2+r^2)^{\frac{1}{2}}}\right]dx$$
$$-\int_r^s \frac{300Q}{Rs^2}\left[1+\frac{x}{(x^2+s^2)^{\frac{1}{2}}}\right]dx \text{ volts/cm.} \qquad (15)$$

Thus the total space charge field at S is

$$E_s = E_{s1}+E_{s3}-E_{s2}$$
$$= \frac{300Q}{Rs^2}\left[r\ln\left\{\left(R^2+\frac{r^4}{s^2}\right)^{\frac{1}{2}}-\frac{r^2}{s}\right\}-r\ln\left\{\frac{r}{s}(r^2+s^2)^{\frac{1}{2}}-\frac{r^2}{s}\right\}\right.$$
$$\left.+R+r-2s-(R^2+s^2)^{\frac{1}{2}}+(r^2+s^2)^{\frac{1}{2}}\right] \text{ volts/cm.}$$

which is equation (1).

References

Allibone, T. E. 1937 *J. Instn Elect. Engrs*, **81**, 841.
Allibone, T. E. 1938 *J. Instn Elect. Engrs*, **82**, 513.
Allibone, T. E. 1948 *Nature, Lond.*, **161**, 970.
Allibone, T. E., Hawley, W. G. & Perry, F. R. 1934 *J. Instn Elect. Engrs*, **75**, 670.
Allibone, T. E. & Meek, J. M. 1938 *Proc. Roy. Soc.* A, **166**, 97.
American Institute of Electrical Engineers Standard no. 4, 1940.
Baatz, H. & Fischer, A. 1961 *Trans. Amer. Inst. Elect. Engrs*, **80**, pt. III, 618 (Discussions).
Bellaschi, P. L. & Teague, W. L. 1934 *Elect. Engng*, **53**, 1638.
Brago, E. N. & Stekolnikov, I. S. 1958 *Izv. Akad. Nauk SSSR O.T.N.* **11**, 50.
British Standard 923, 1940.
British Standard 358, 1960.

PHILOSOPHICAL TRANSACTIONS OF THE ROYAL SOCIETY A MATHEMATICAL, PHYSICAL & ENGINEERING SCIENCES

Chalmers, J. A. 1957 *Atmospheric electricity*. Oxford: Clarendon Press.
Dyson, J., Hemmings, R. F. & Waters, R. T. 1960 *Proc. Fifth International Congress on High-speed Photography*. Washington.
Gorev, A. A., Zalesky, A. M. & Riabov, B. M. 1948 *C.I.G.R.E.* Paper no. **142**.
Komelkov, V. 1947 *Dokl. Akad. Nauk SSSR*, **68**, 57.
Kuffel, E. 1959 *Proc. Instn Elect. Engrs*, **106**, pt. C, 133.
Loeb, L. B. 1935 *Phys. Rev.* **48**, 684.
Loeb, L. B. 1939 *Fundamental processes of electrical discharges in gases*. New York: Wiley.
Loeb, L. B. 1959 *Phys. Rev.* **113**, 7.
Loeb, L. B., Kip, A. F. Hudson, G. G., Bennett, W. H. 1941 *Phys. Rev.* **60**, 714.
Muschlitz, E. E. 1959 *Proc. Fourth Int. Conf. on Ionization Phenomena in Gases*. North-Holland Publishing Company.
Park, J. H. & Cones, N. H. 1956 *Bur. Stand. J. Res., Wash.*, **56**, 201.
Saxe, R. F. & Meek, J. M. 1955 *Proc. Instn Elect. Engrs*, **102**, pt. C, 221.
Stekolnikov, I. S. & Bagirov, M. A. 1954 *Zh. Eksp. Teor. Fiz.* **27**, no. 2 (8), 189.
Trichel, G. W. 1938 *Phys. Rev.* **54**, 1078.
Waters, R. T. 1962 *Gas discharges and the electricity supply industry*. London: Butterworths.
Waters, R. T. & Jones, R. E. 1959 *Proc. Fourth Int. Conf. on Ionization Phenomena in Gases*. North-Holland Publishing Company.
Waters, R. T. & Jones, R. E. 1961 *Proc. Fifth Int. Conf. on Ionization Phenomena in Gases*. North-Holland Publishing Company.
Waters, R. T. & Jones, R. E. 1962 *Proc. Instn Elect. Engrs*, **109**, pt. A, 144.

PHILOSOPHICAL TRANSACTIONS OF THE ROYAL SOCIETY A MATHEMATICAL, PHYSICAL & ENGINEERING SCIENCES

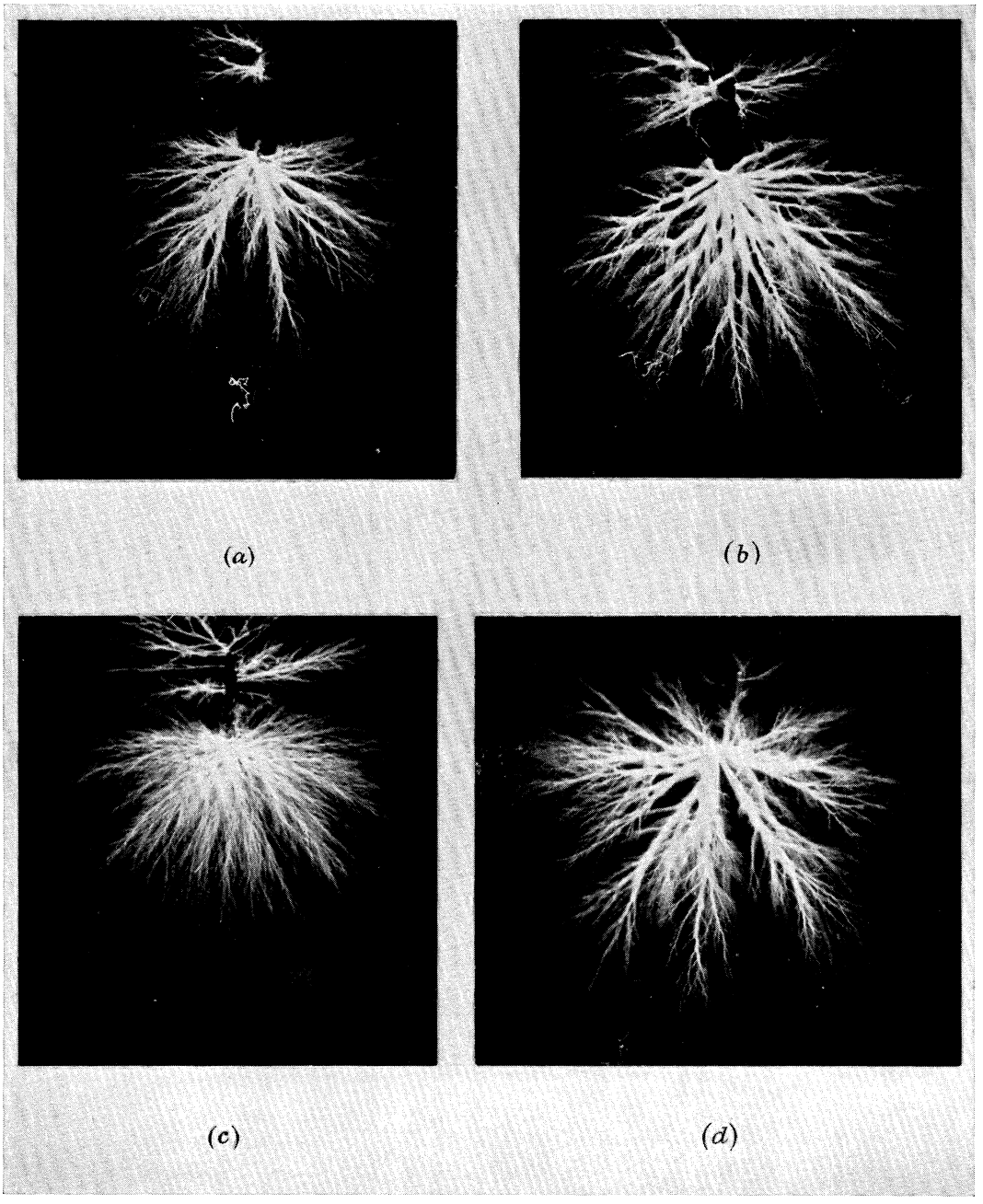

FIGURE 1. Impulse corona discharge at a rod-anode. (*a*) 190 kV crest voltage, 0·50 μs wave front, corona extent 17·7 cm; (*b*) 190 kV crest voltage, 0·20 μs wave front, corona extent 20·2 cm; (*c*) 270 kV crest voltage, 0·50 μs wave front, corona extent 20·7 cm; (*d*) 270 kV crest voltage, 0·20 μs wave front, corona extent 29·0 cm.

(*Facing p.* 212)

PHILOSOPHICAL TRANSACTIONS OF THE ROYAL SOCIETY A MATHEMATICAL, PHYSICAL & ENGINEERING SCIENCES

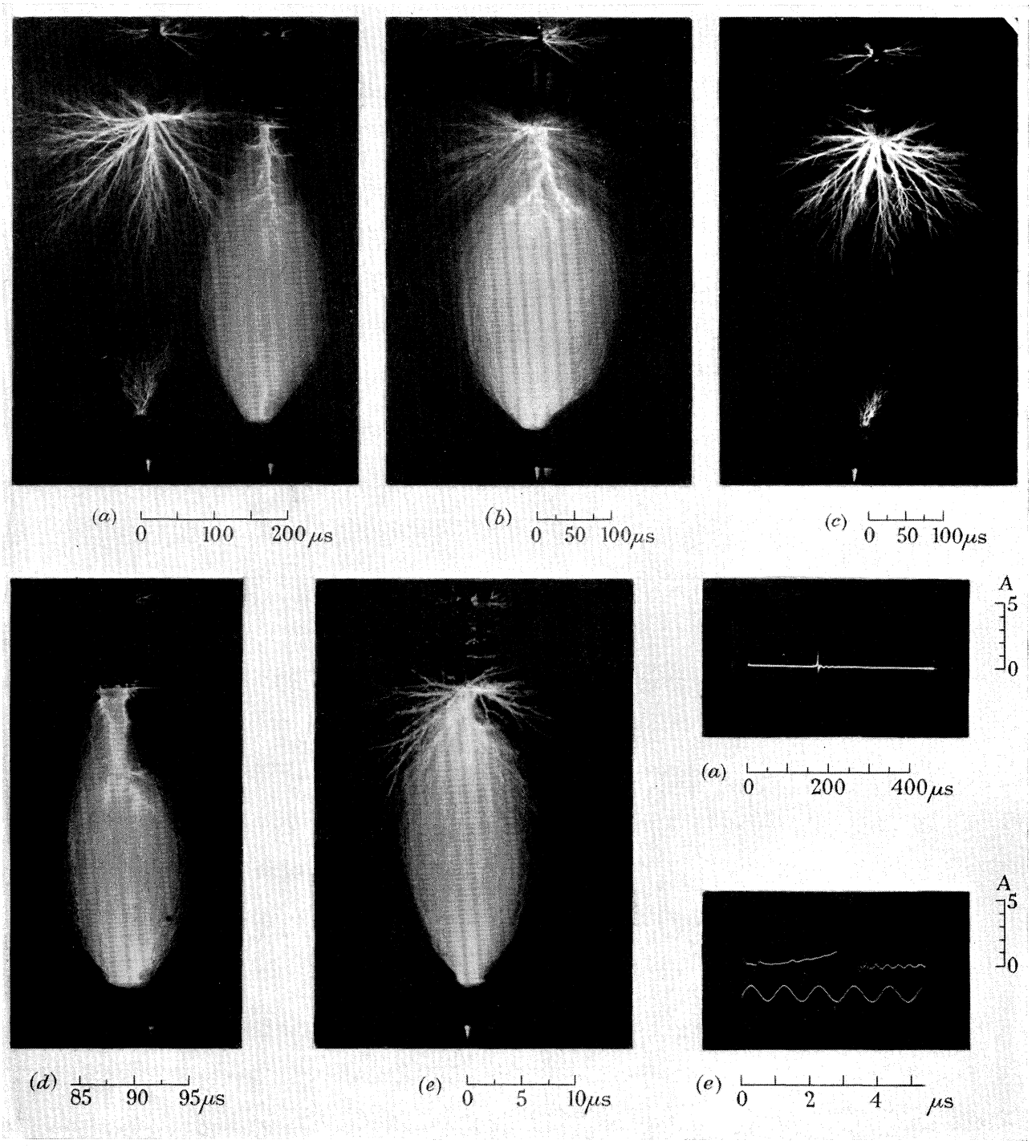

FIGURE 4. Time-resolved photographs of arrested breakdown in a 40 cm rod/rod gap; wave shape 0·50/2000 μs. (*a*) to (*d*) 275 kV crest voltage; (*e*) 310 kV crest voltage.

PHILOSOPHICAL TRANSACTIONS OF THE ROYAL SOCIETY A MATHEMATICAL, PHYSICAL & ENGINEERING SCIENCES

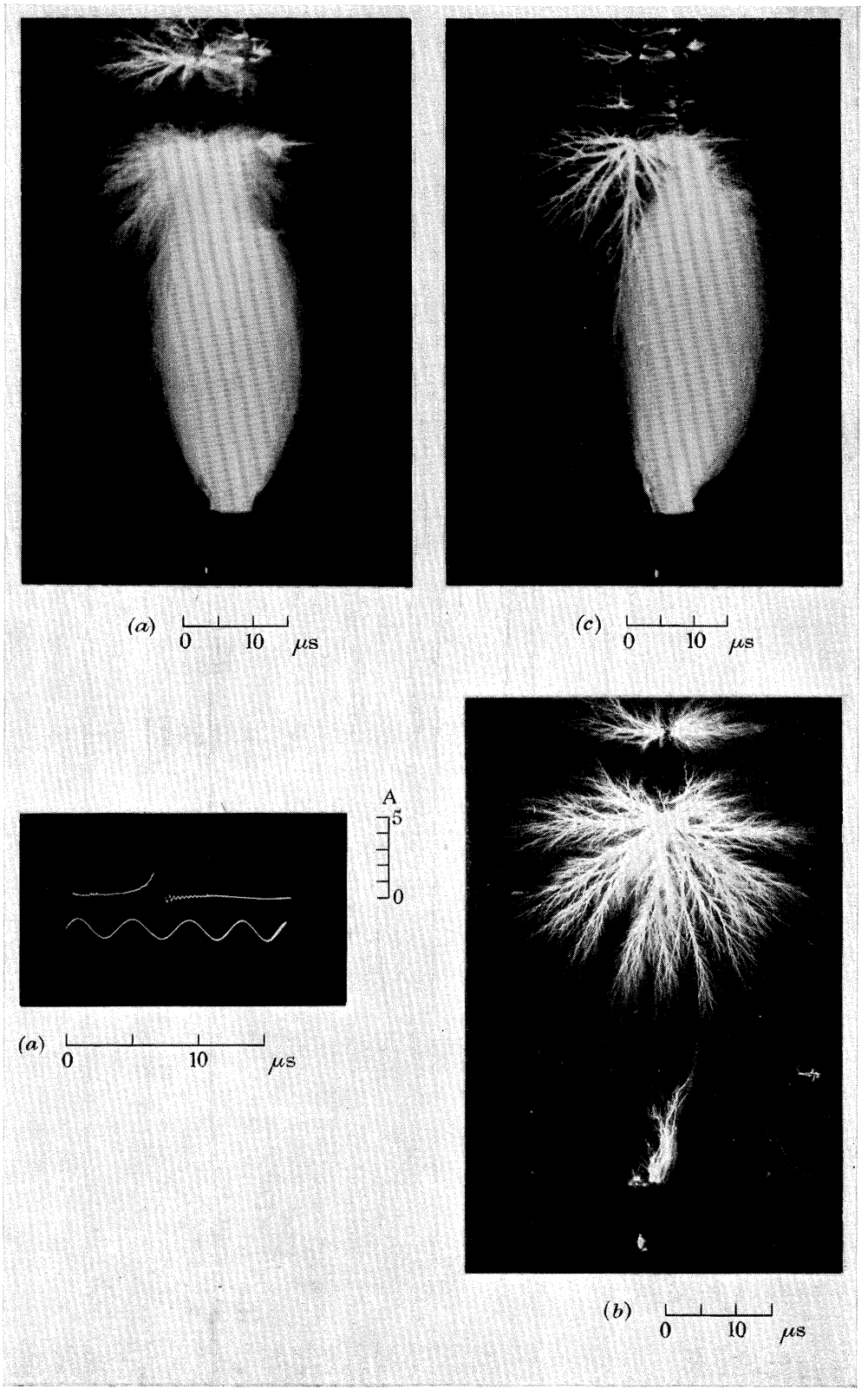

FIGURE 5. Time-resolved photographs of arrested breakdown in a 55 cm rod/rod gap for 380 kV crest voltage; wave shape 0·50/2000 μs.

PHILOSOPHICAL TRANSACTIONS OF THE ROYAL SOCIETY A MATHEMATICAL, PHYSICAL & ENGINEERING SCIENCES

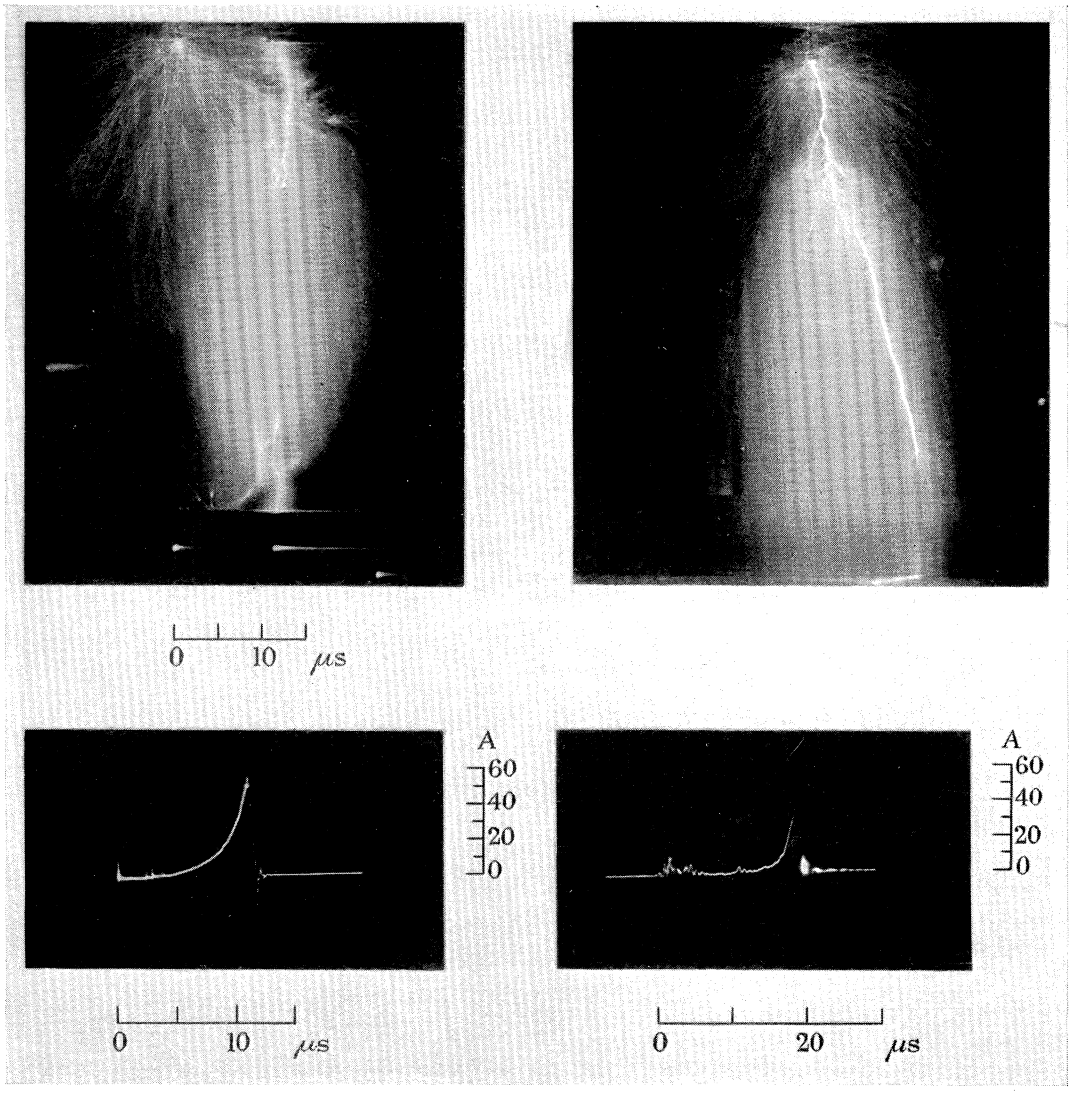

FIGURE 6 FIGURE 11

FIGURE 6. Time-resolved photograph of arrested breakdown in a 170 cm rod/rod gap for 970 kV; wave shape 0·50/2000 μs.

FIGURE 11. Still photograph of arrested breakdown in a 2 m rod/plane gap for 950 kV crest voltage; wave shape 0·50/2000 μs.

PHILOSOPHICAL TRANSACTIONS OF THE ROYAL SOCIETY A MATHEMATICAL, PHYSICAL & ENGINEERING SCIENCES

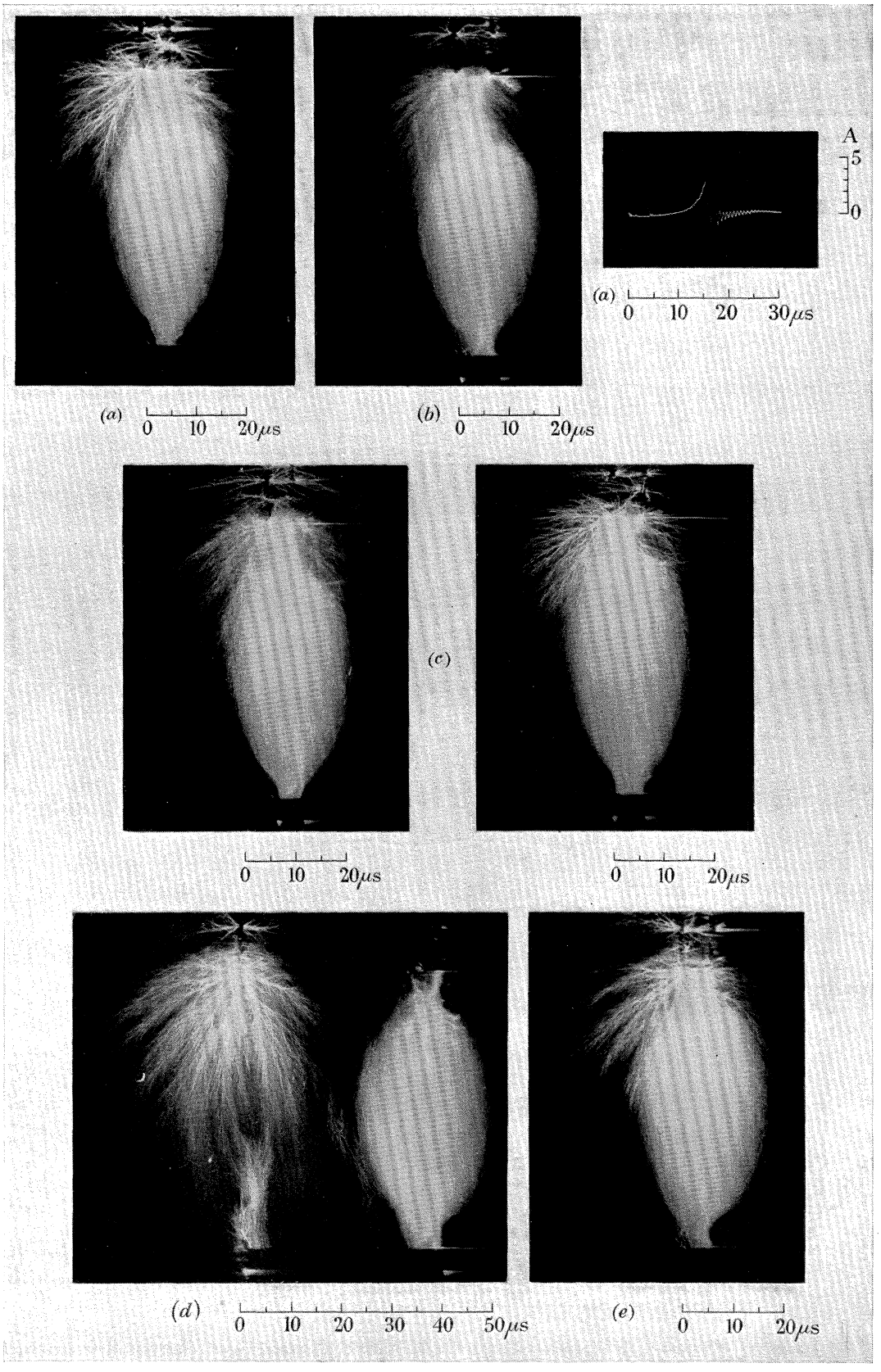

FIGURE 9. Time-resolved photographs of arrested breakdown in a 76·2 cm rod/rod gap.

	(*a*)	(*b*)	(*c*)	(*d*)	(*e*)
crest voltage (kV)	500	475	500	500	515
wave shape (μs)	0·50/2000	0·50/2000	0·35/2000	0·20/2000	0·20/2000

PHILOSOPHICAL TRANSACTIONS OF THE ROYAL SOCIETY A MATHEMATICAL, PHYSICAL & ENGINEERING SCIENCES

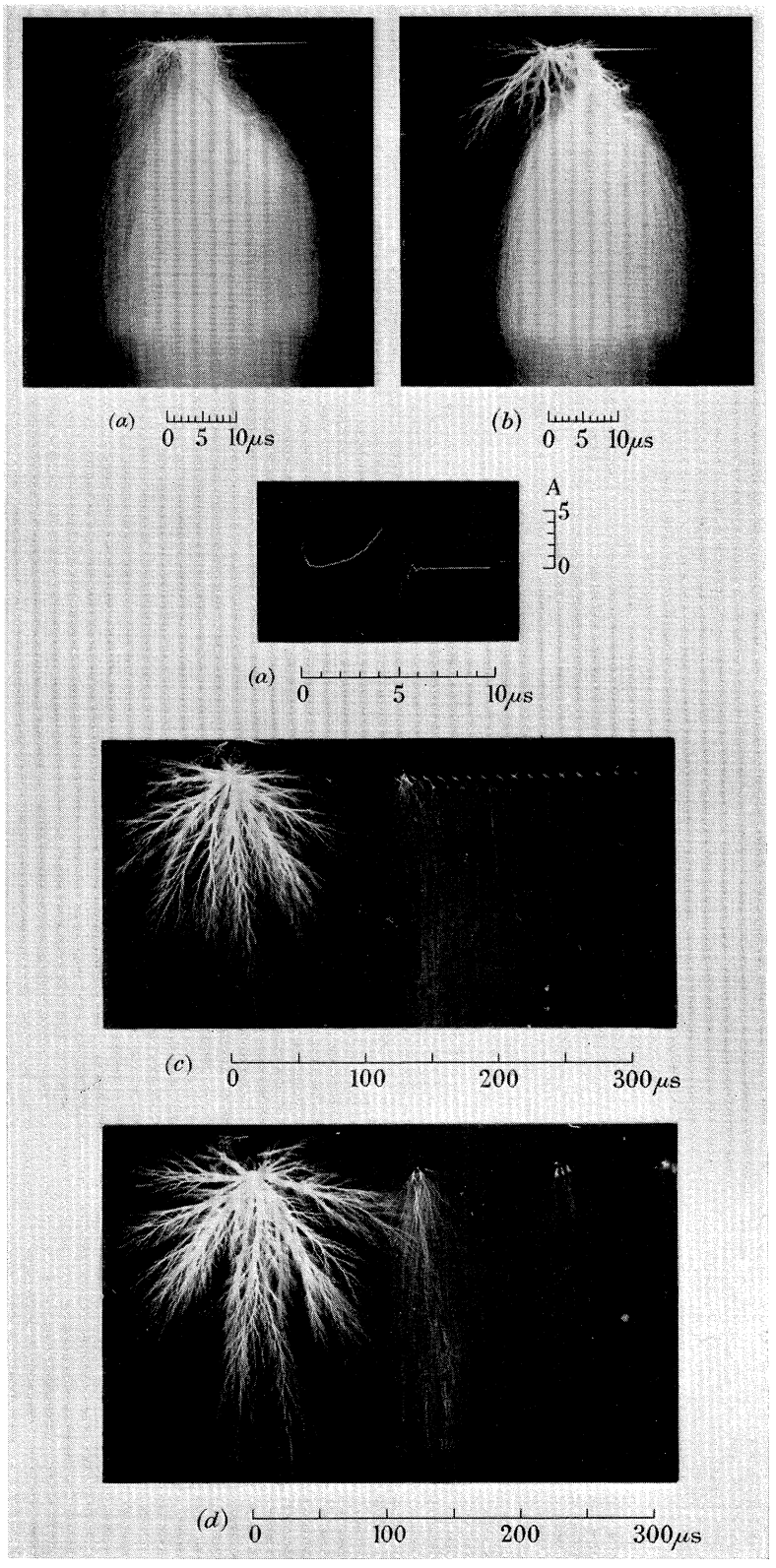

FIGURE 12. Time-resolved photographs of discharges in a 40 cm rod/plane gap for 250 kV crest voltage; wave shape 0·50/2000 μs. (*a*) and (*b*) arrested; (*c*) and (*d*) no breakdown.

PHILOSOPHICAL TRANSACTIONS OF THE ROYAL SOCIETY A MATHEMATICAL, PHYSICAL & ENGINEERING SCIENCES

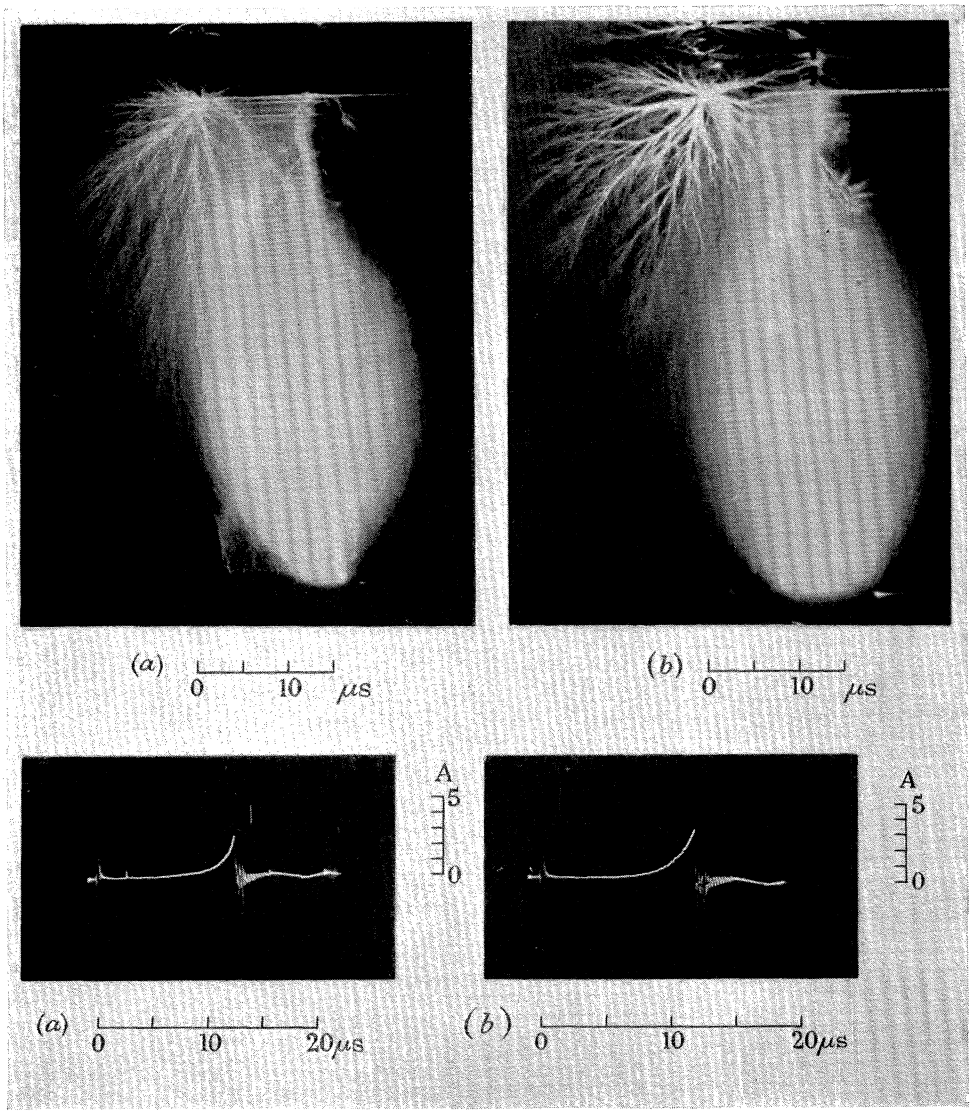

FIGURE 14. Time-resolved photographs of arrested breakdown in 80 cm rod/sphere gaps; wave shape 0·50/2000 μs. (*a*) 12·5 cm diameter sphere, 480 kV crest voltage; (*b*) 25 cm diameter sphere, 460 kV crest voltage.

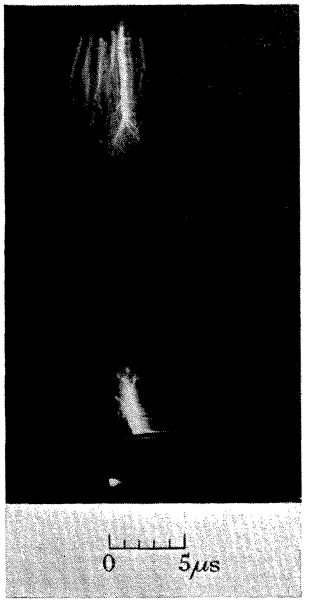

FIGURE 15. Time-resolved photograph of arrested breakdown in a 75 cm diameter sphere/rod gap at 900 kV crest voltage; gap spacing 65 cm; wave shape 0·50/2000 μs.

PHILOSOPHICAL TRANSACTIONS OF THE ROYAL SOCIETY A MATHEMATICAL, PHYSICAL & ENGINEERING SCIENCES

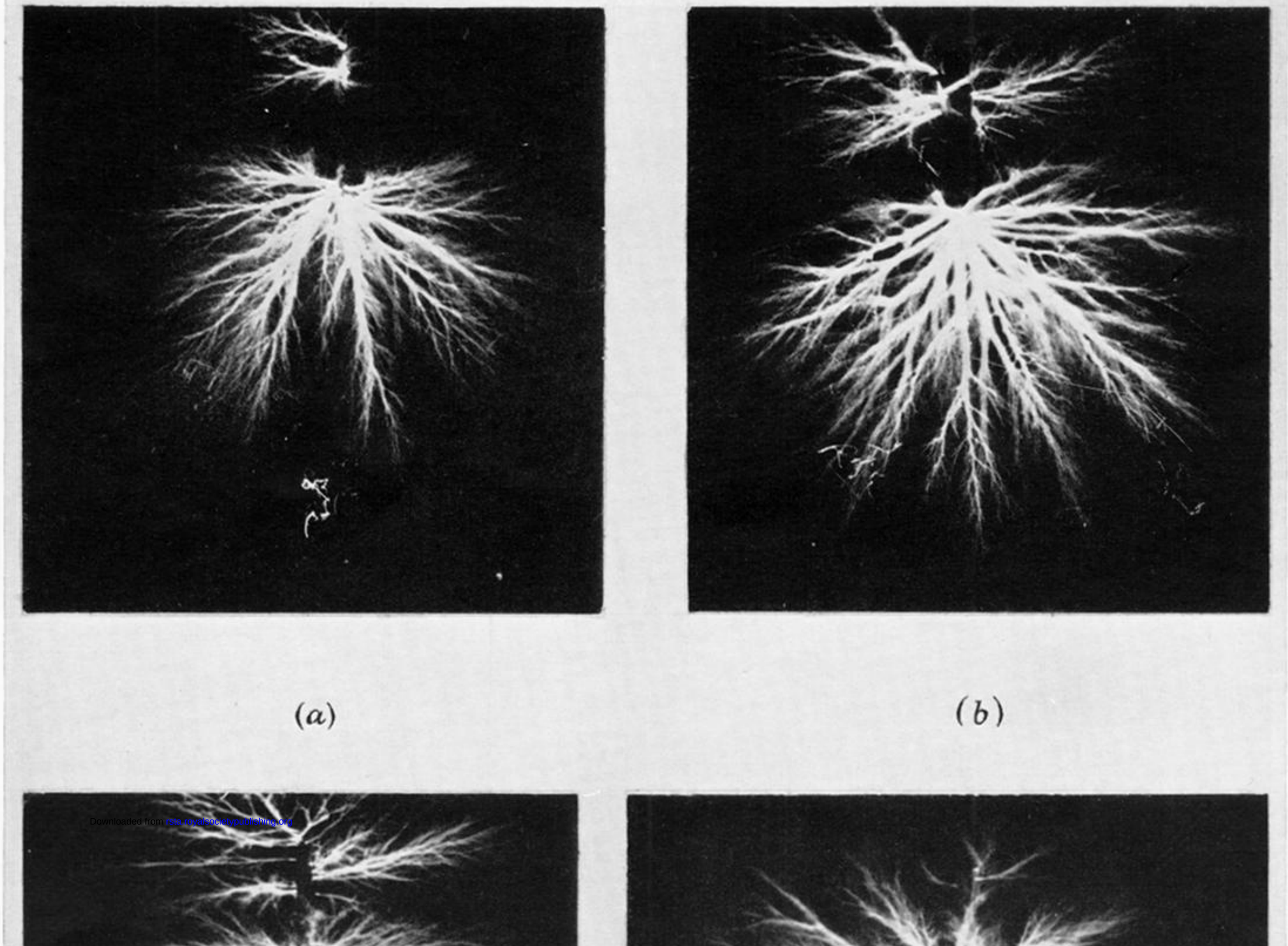

FIGURE 1. Impulse corona discharge at a rod-anode. (*a*) 190 kV crest voltage, 0·50 μs wave front, corona extent 17·7 cm; (*b*) 190 kV crest voltage, 0·20 μs wave front, corona extent 20·2 cm; (*c*) 270 kV crest voltage, 0·50 μs wave front, corona extent 20·7 cm; (*d*) 270 kV crest voltage, 0·20 μs wave front, corona extent 29·0 cm.

FIGURE 4. Time-resolved photographs of arrested breakdown in a 40 cm rod/rod gap; wave shape 0·50/2000 μs. (*a*) to (*d*) 275 kV crest voltage; (*e*) 310 kV crest voltage.

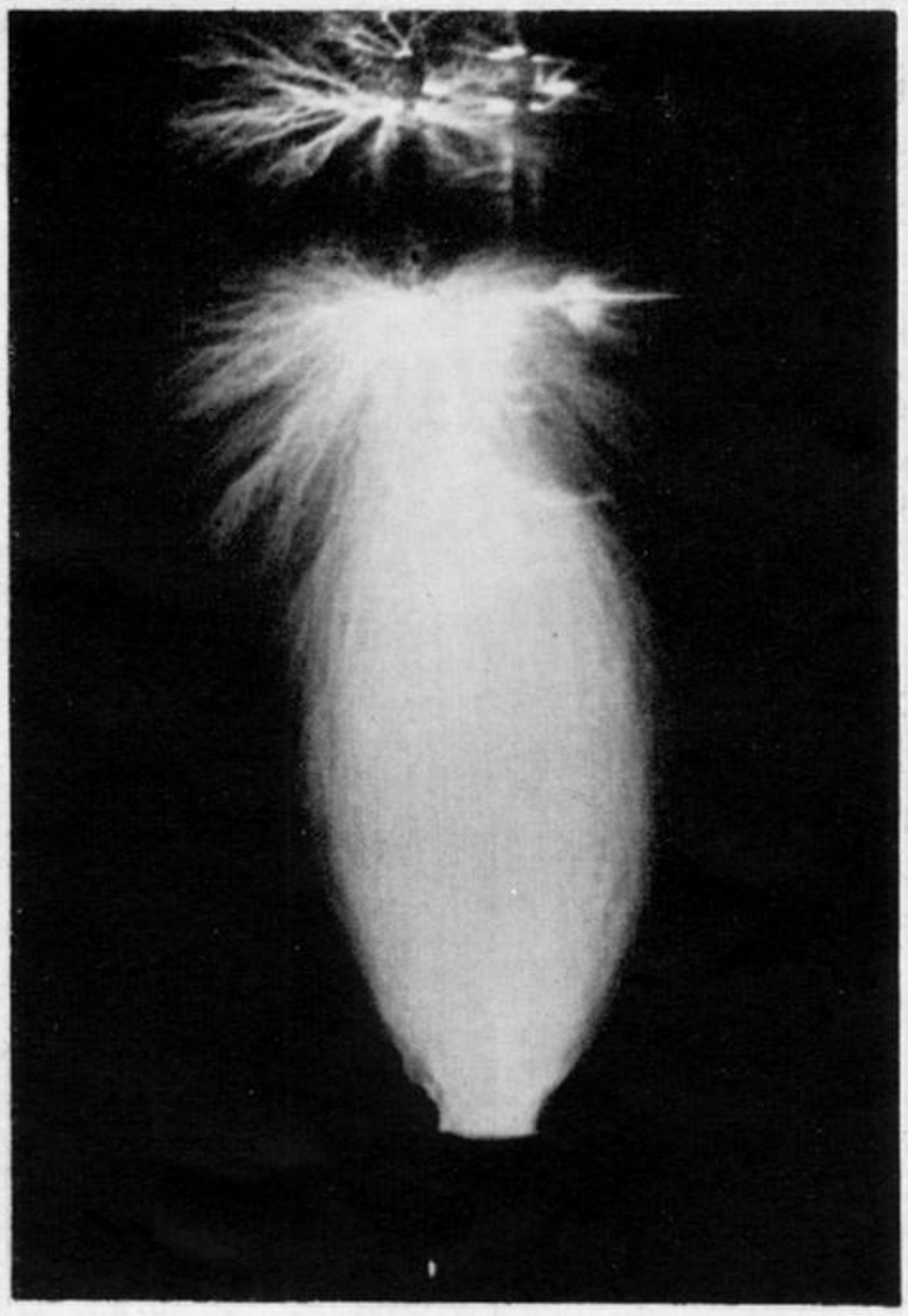

(a) 0 10 μs

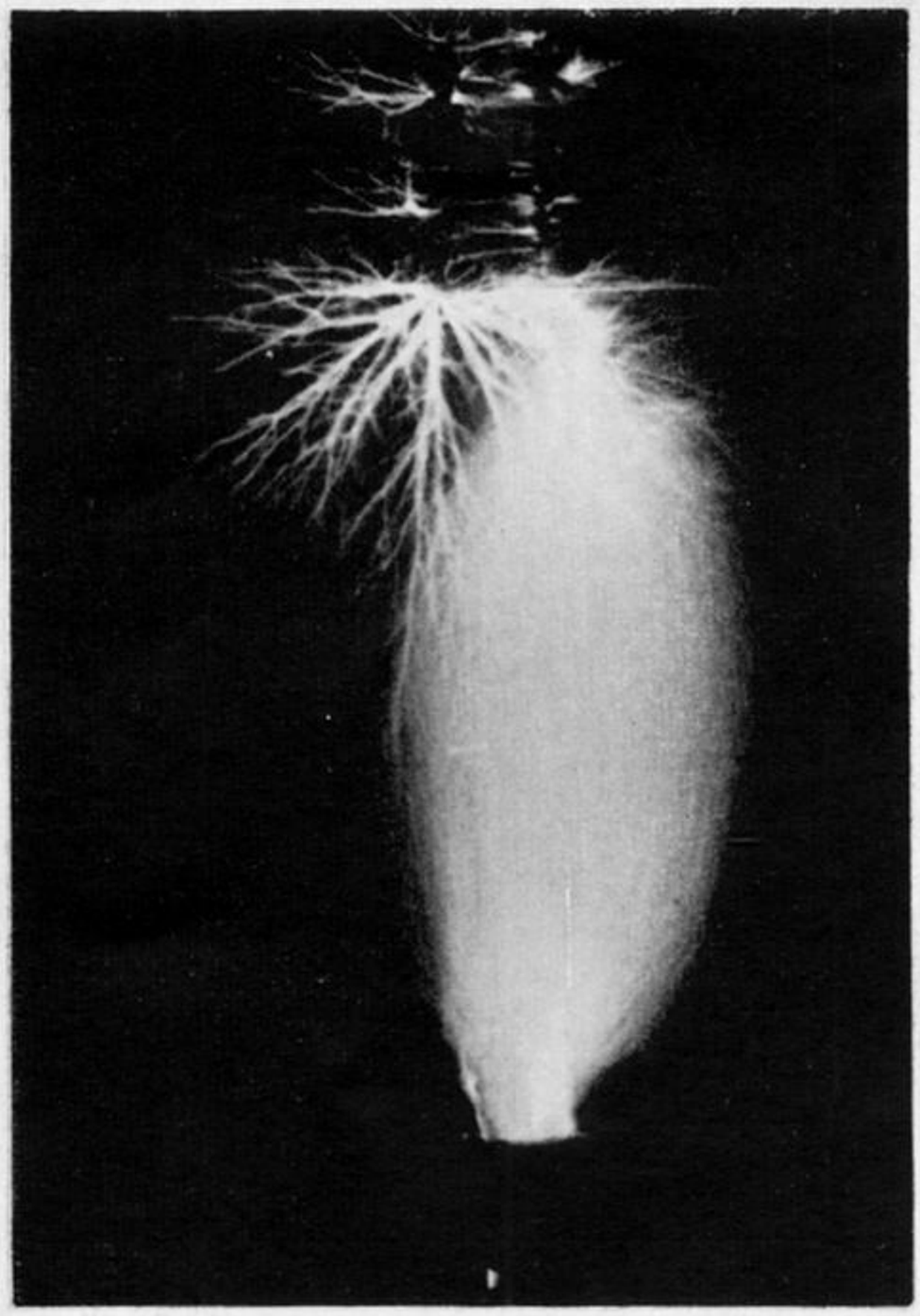

(c) 0 10 μs

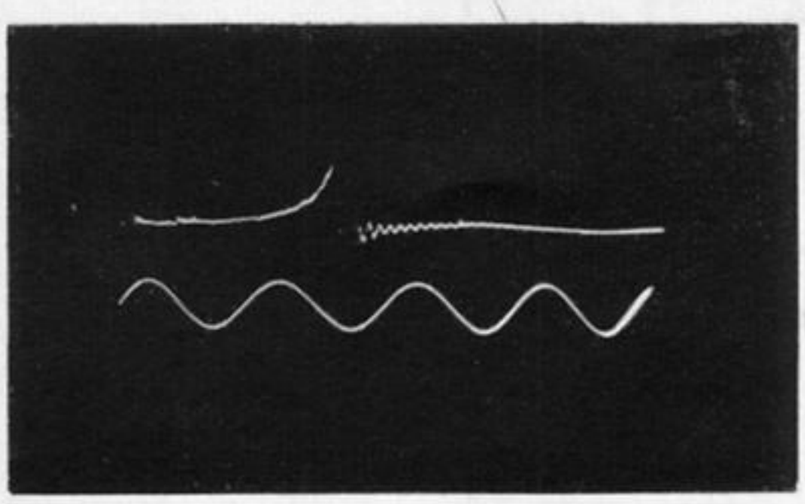

(a) 0 10 μs

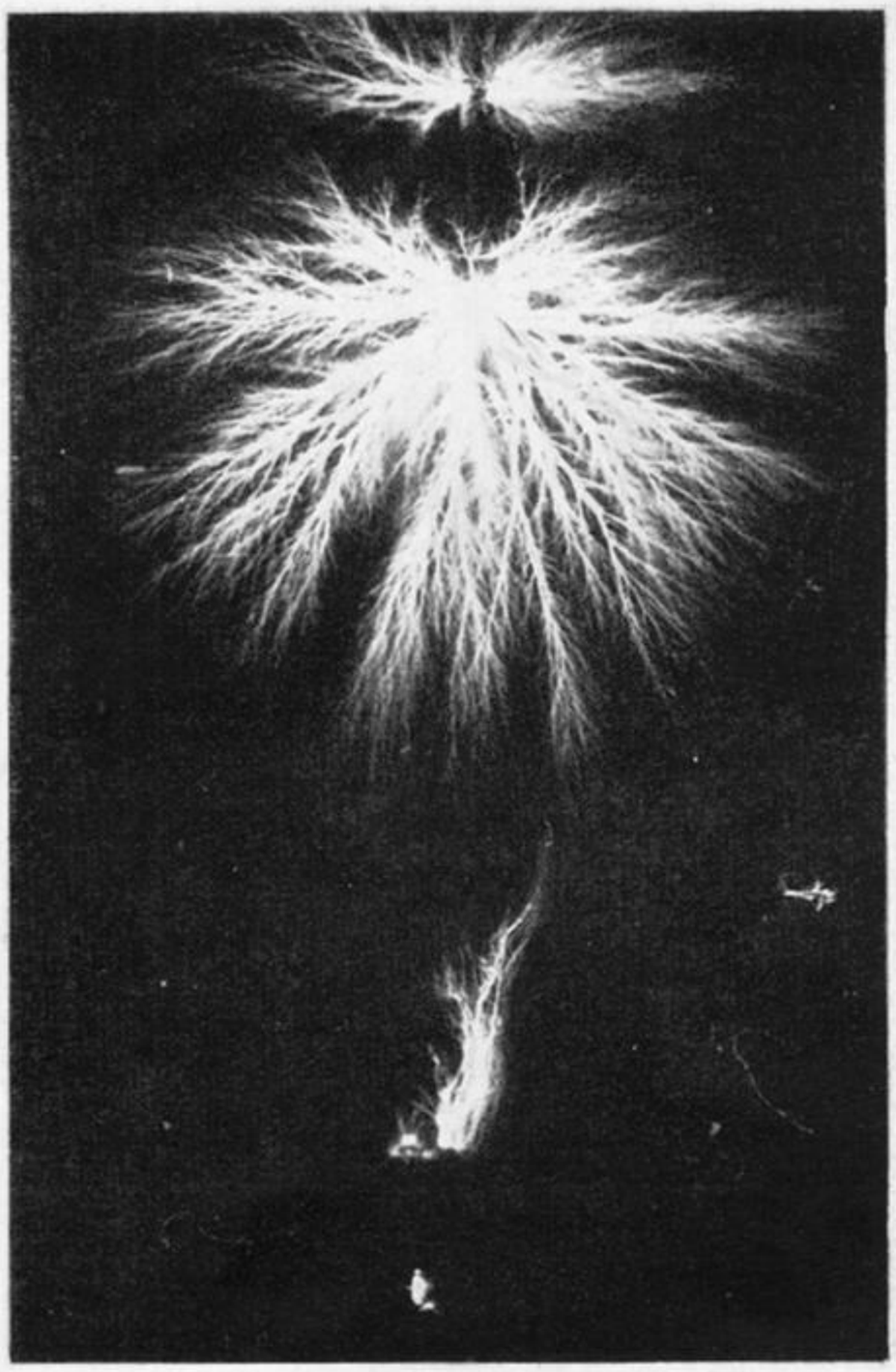

(b) 0 10 μs

FIGURE 5. Time-resolved photographs of arrested breakdown in a 55 cm rod/rod gap for 380 kV crest voltage; wave shape 0·50/2000 μs.

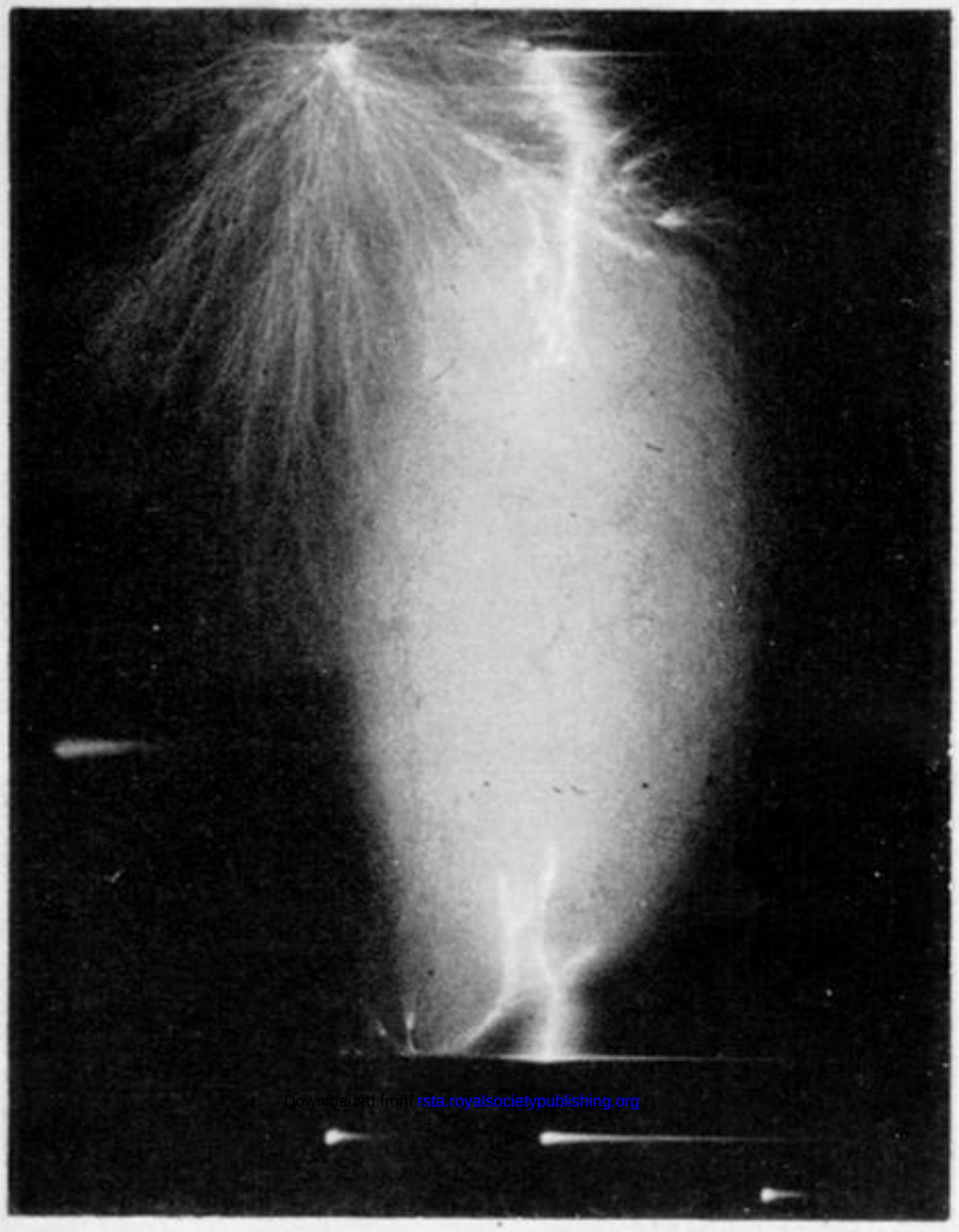

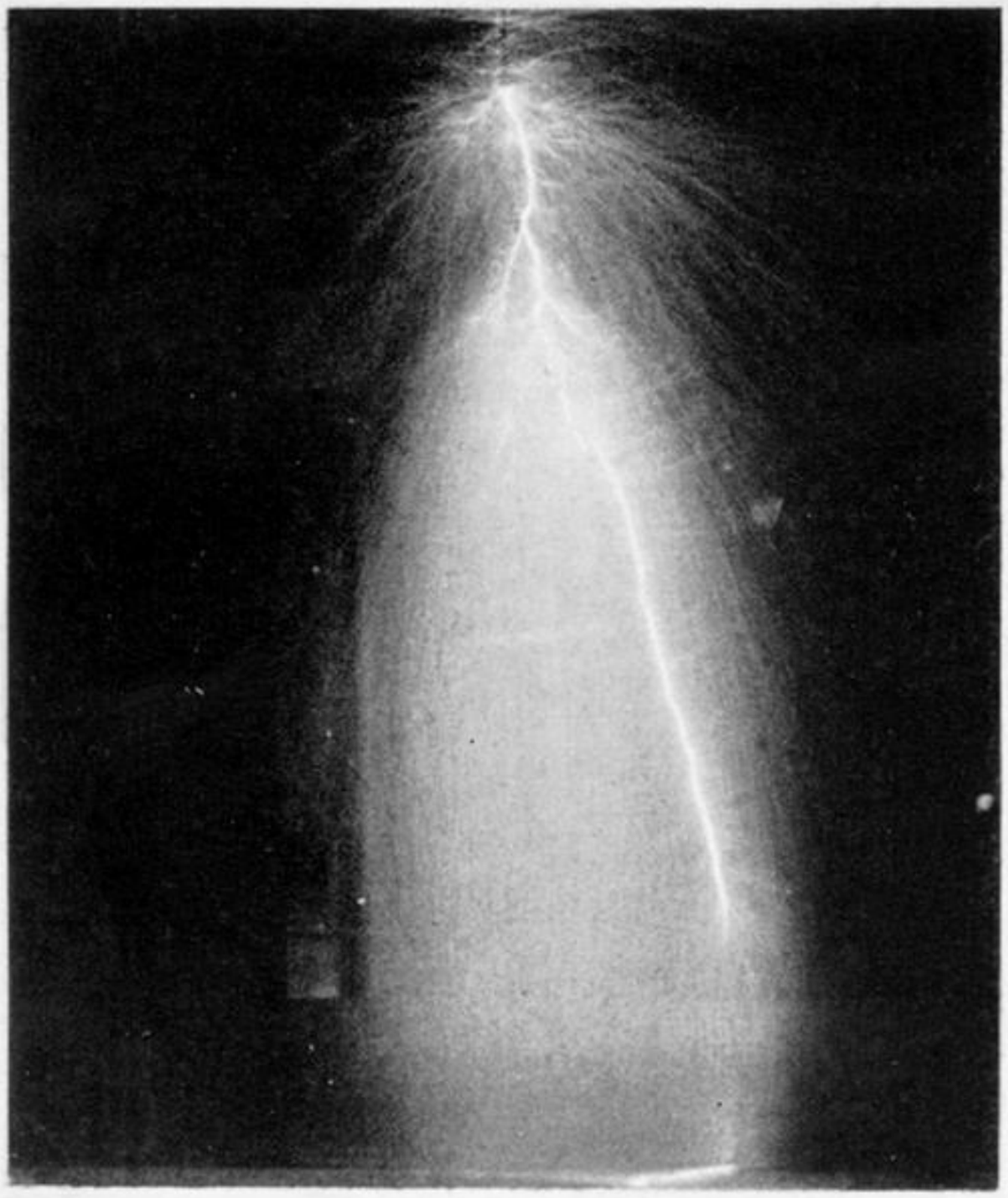

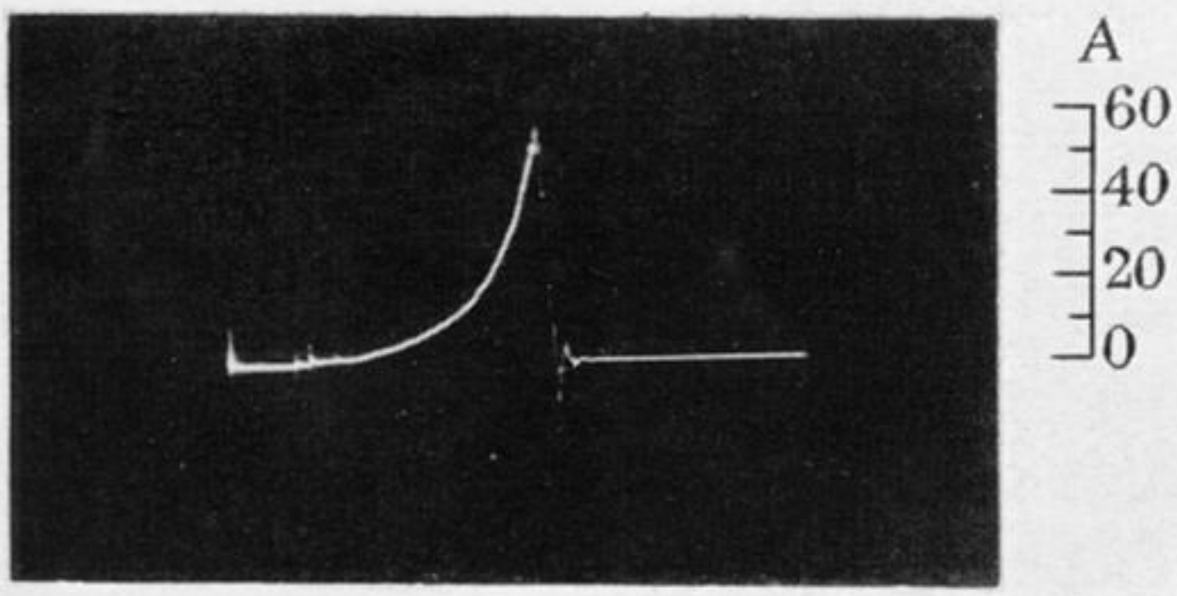

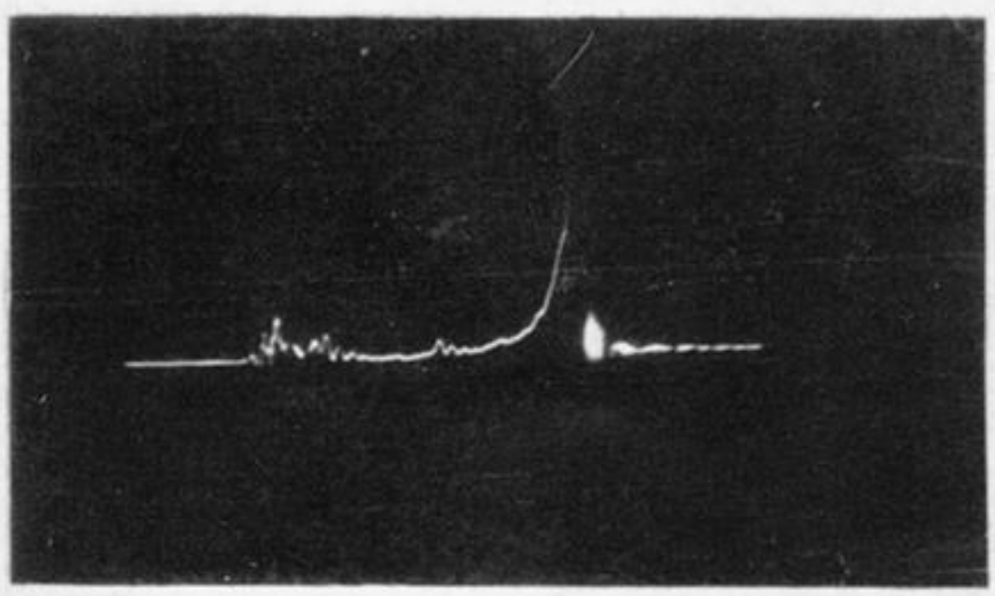

FIGURE 6

FIGURE 11

FIGURE 6. Time-resolved photograph of arrested breakdown in a 170 cm rod/rod gap for 970 kV; wave shape 0·50/2000 μs.

FIGURE 11. Still photograph of arrested breakdown in a 2 m rod/plane gap for 950 kV crest voltage; wave shape 0·50/2000 μs.

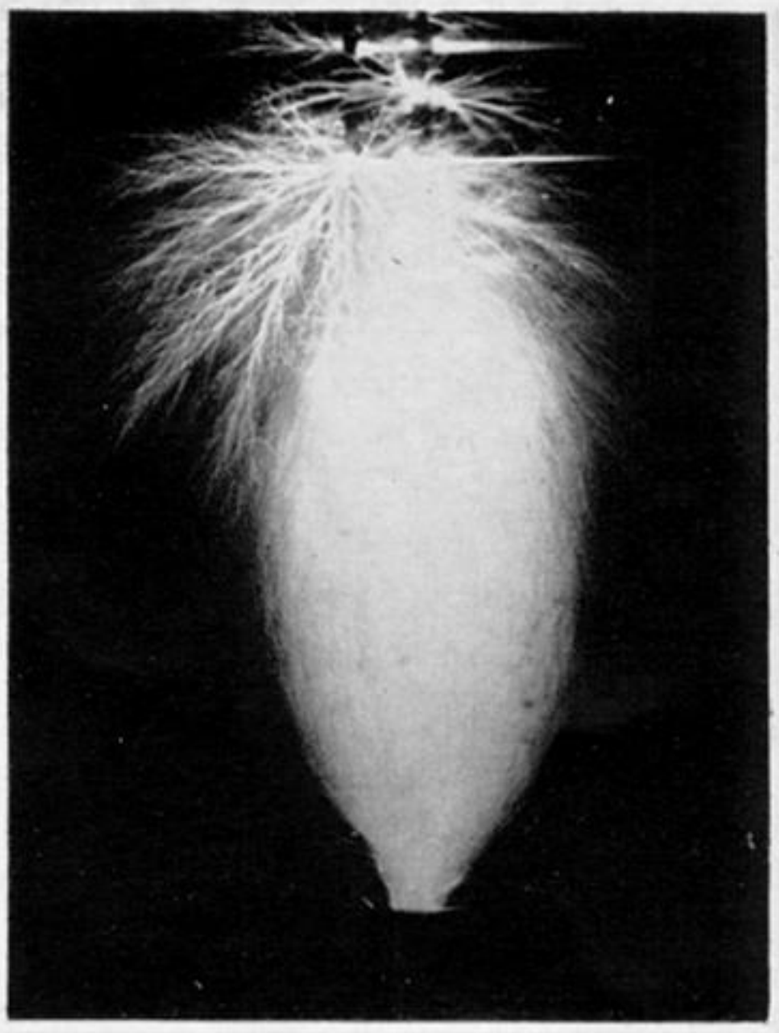

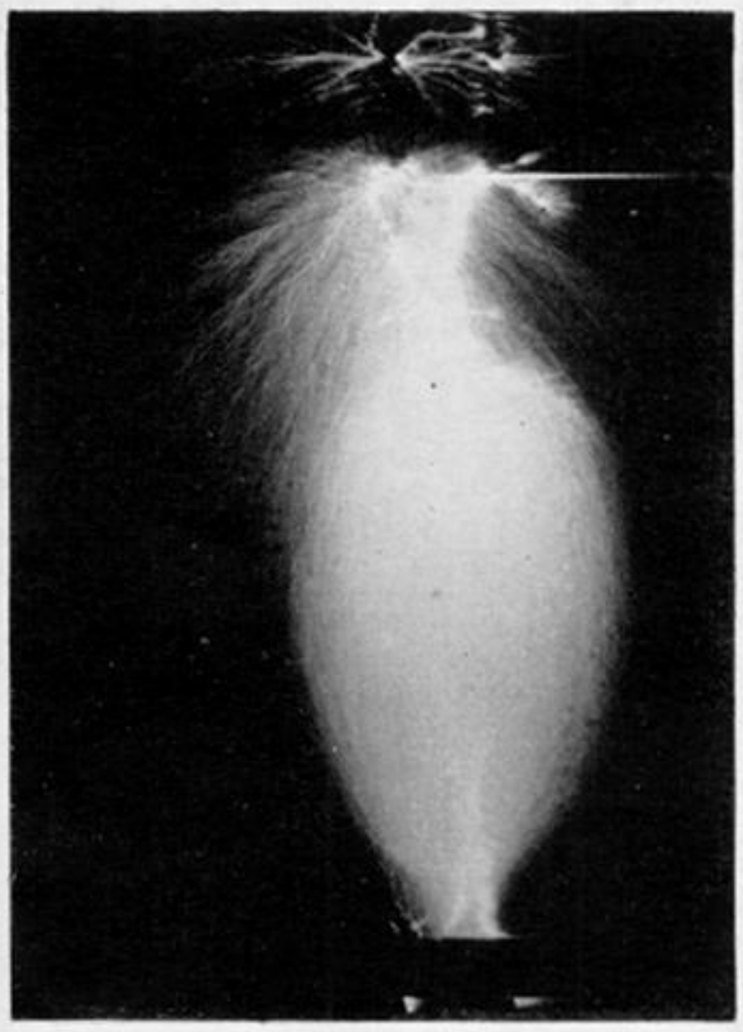

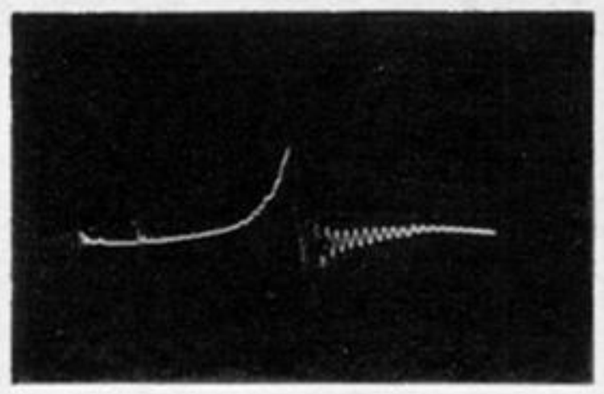

(*a*) 0 10 20 30 μs

(*a*) 0 10 20 μs

(*b*) 0 10 20 μs

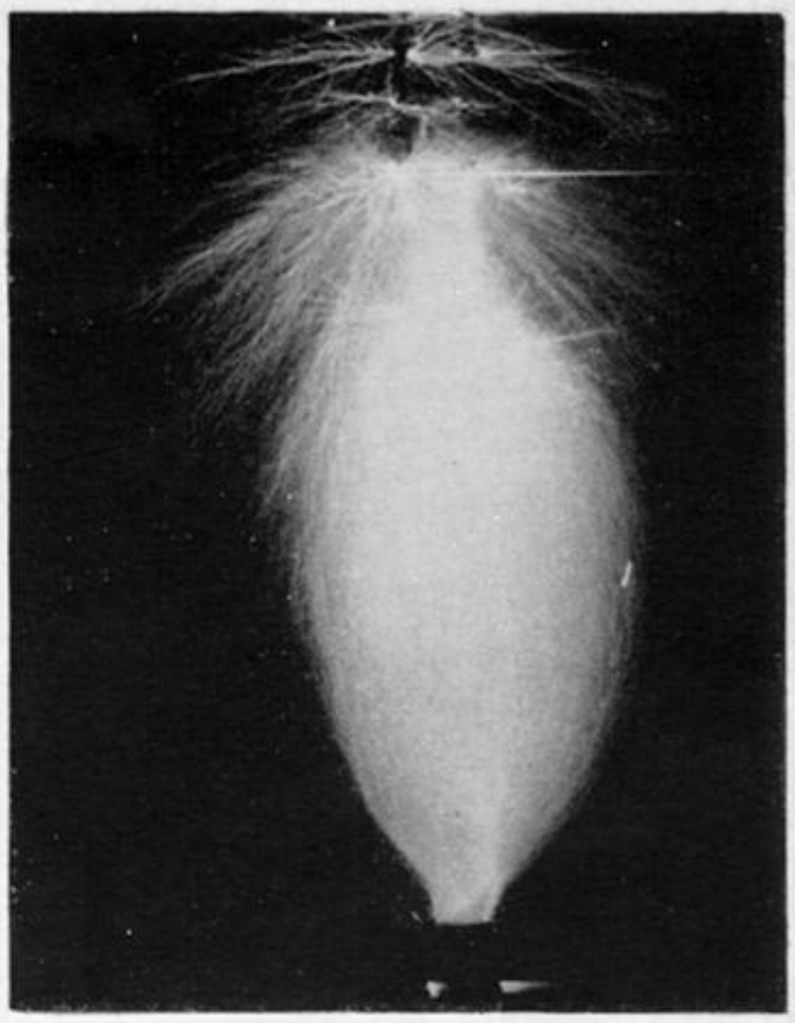

(*c*)

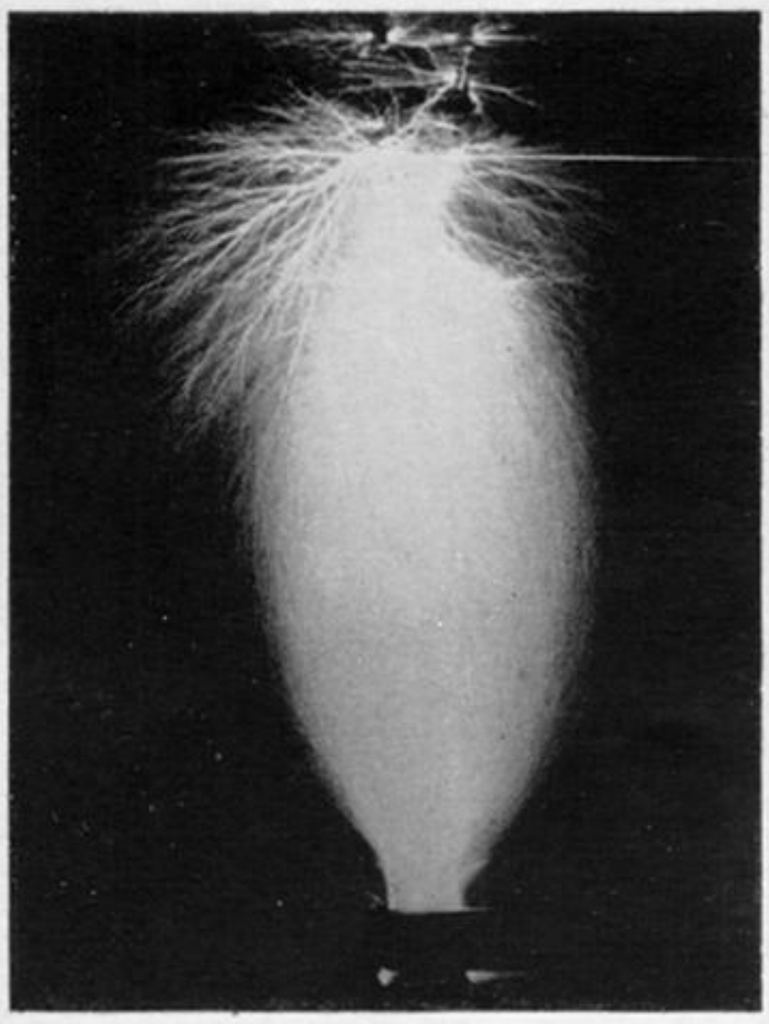

0 10 20 μs

0 10 20 μs

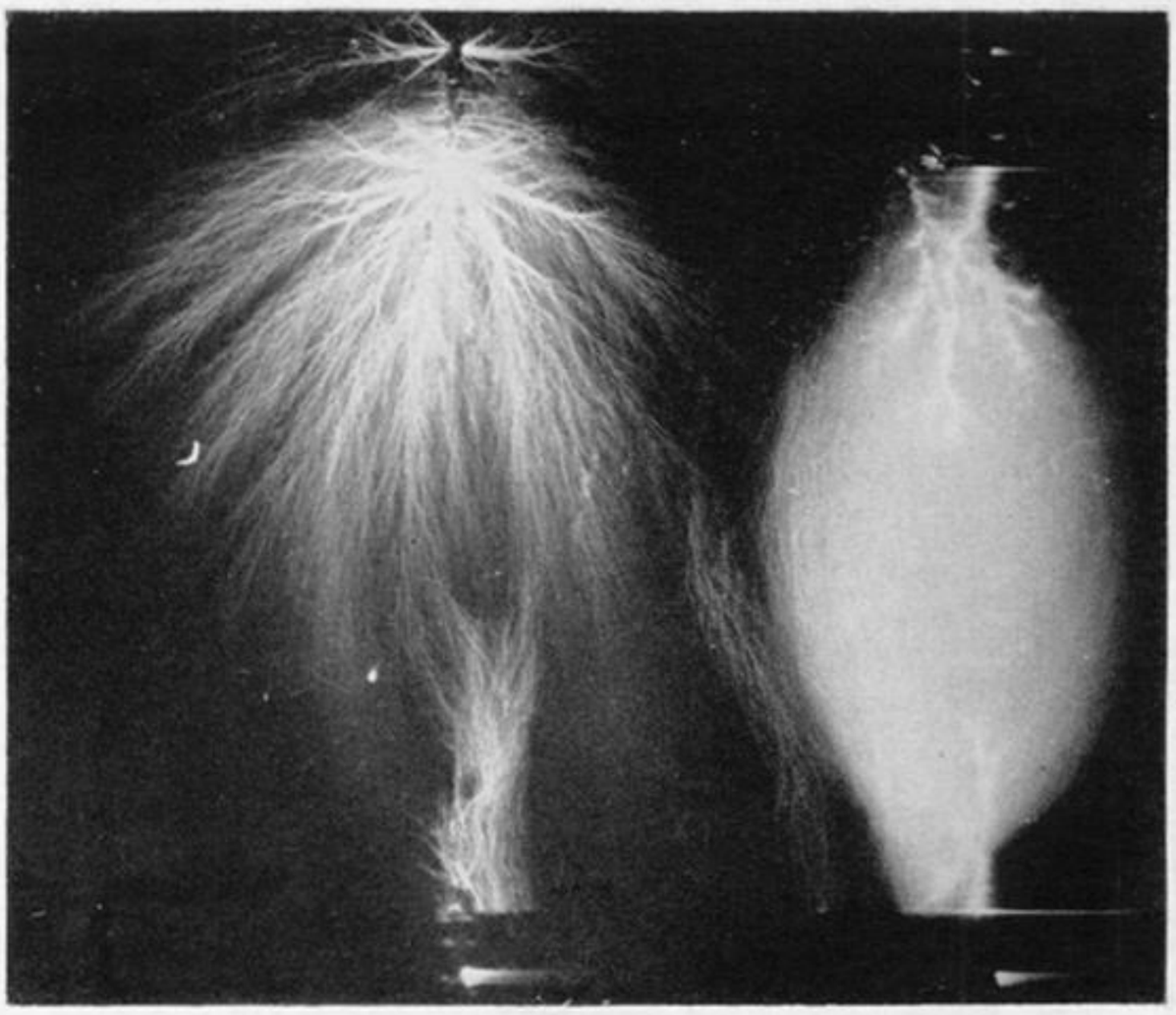

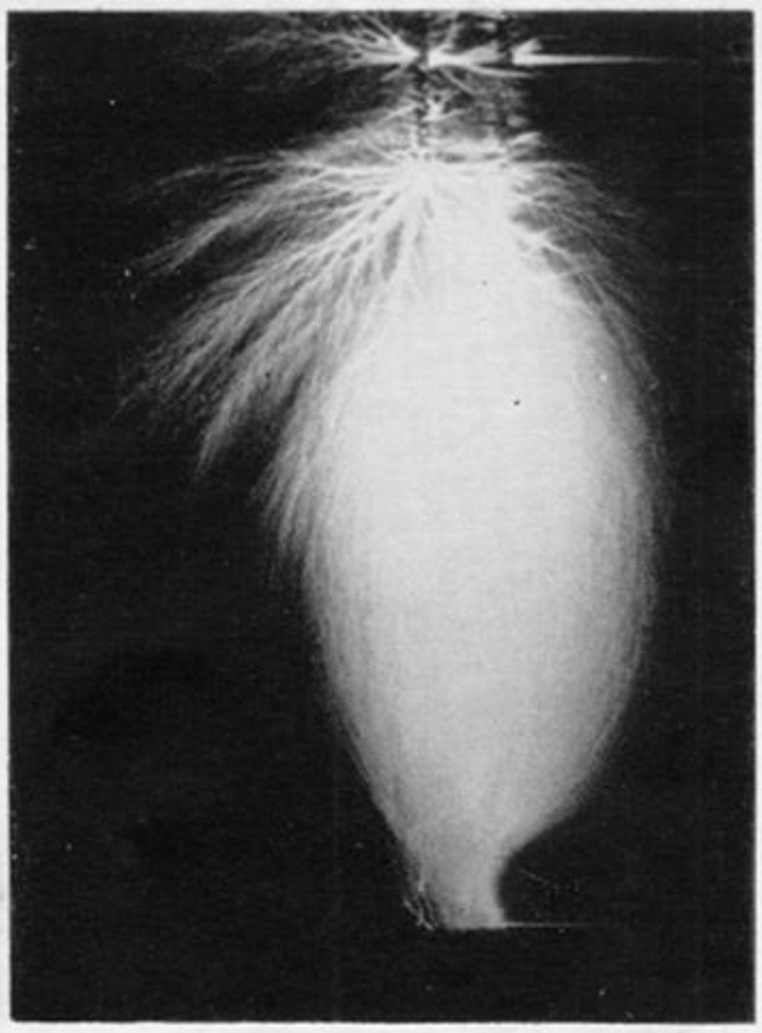

(*d*) 0 10 20 30 40 50 μs

(*e*) 0 10 20 μs

FIGURE 9. Time-resolved photographs of arrested breakdown in a 76·2 cm rod/rod gap.

	(*a*)	(*b*)	(*c*)	(*d*)	(*e*)
crest voltage (kV)	500	475	500	500	515
wave shape (μs)	0·50/2000	0·50/2000	0·35/2000	0·20/2000	0·20/2000

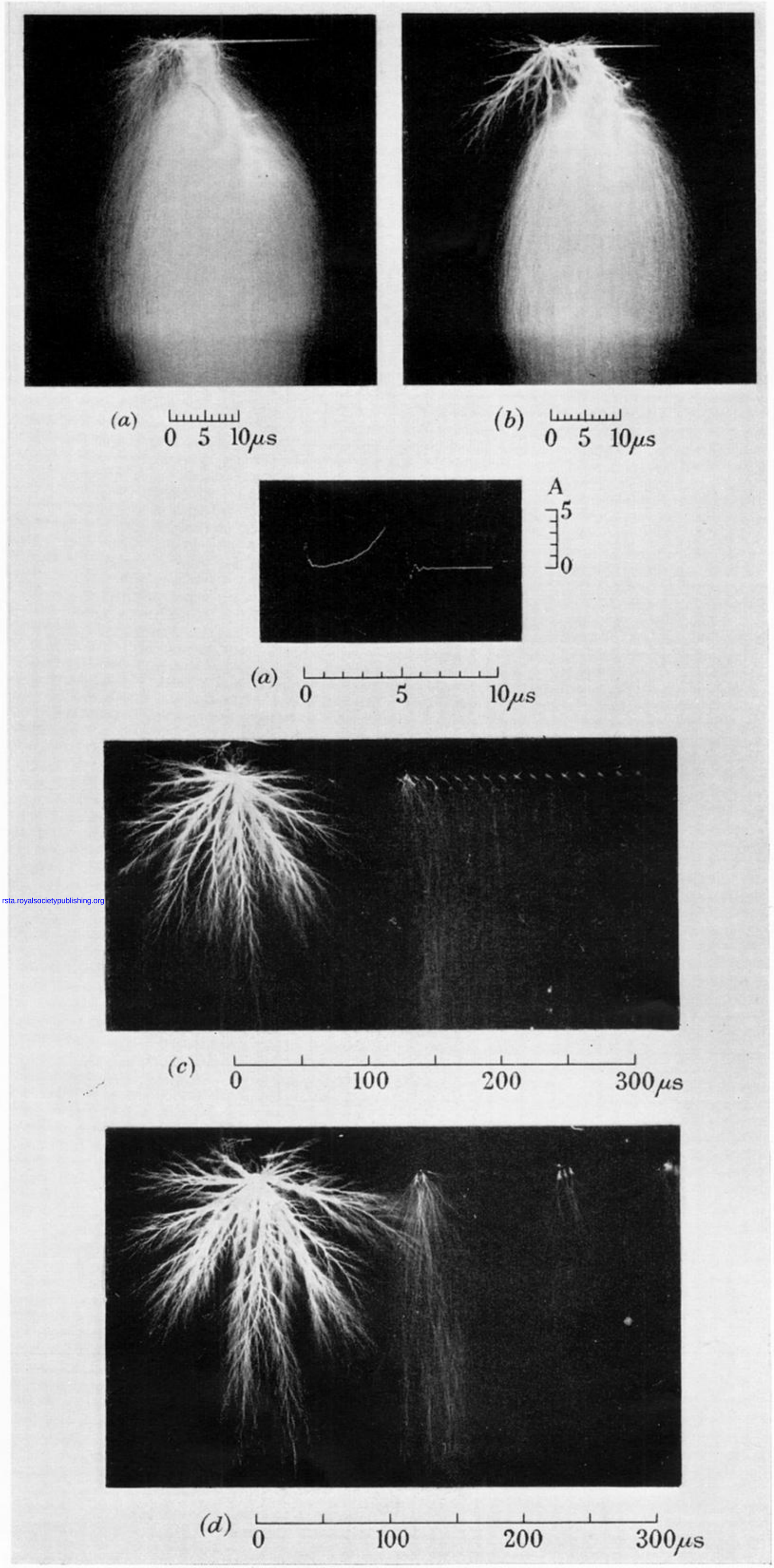

FIGURE 12. Time-resolved photographs of discharges in a 40 cm rod/plane gap for 250 kV crest voltage; wave shape 0·50/2000 μs. (*a*) and (*b*) arrested; (*c*) and (*d*) no breakdown.

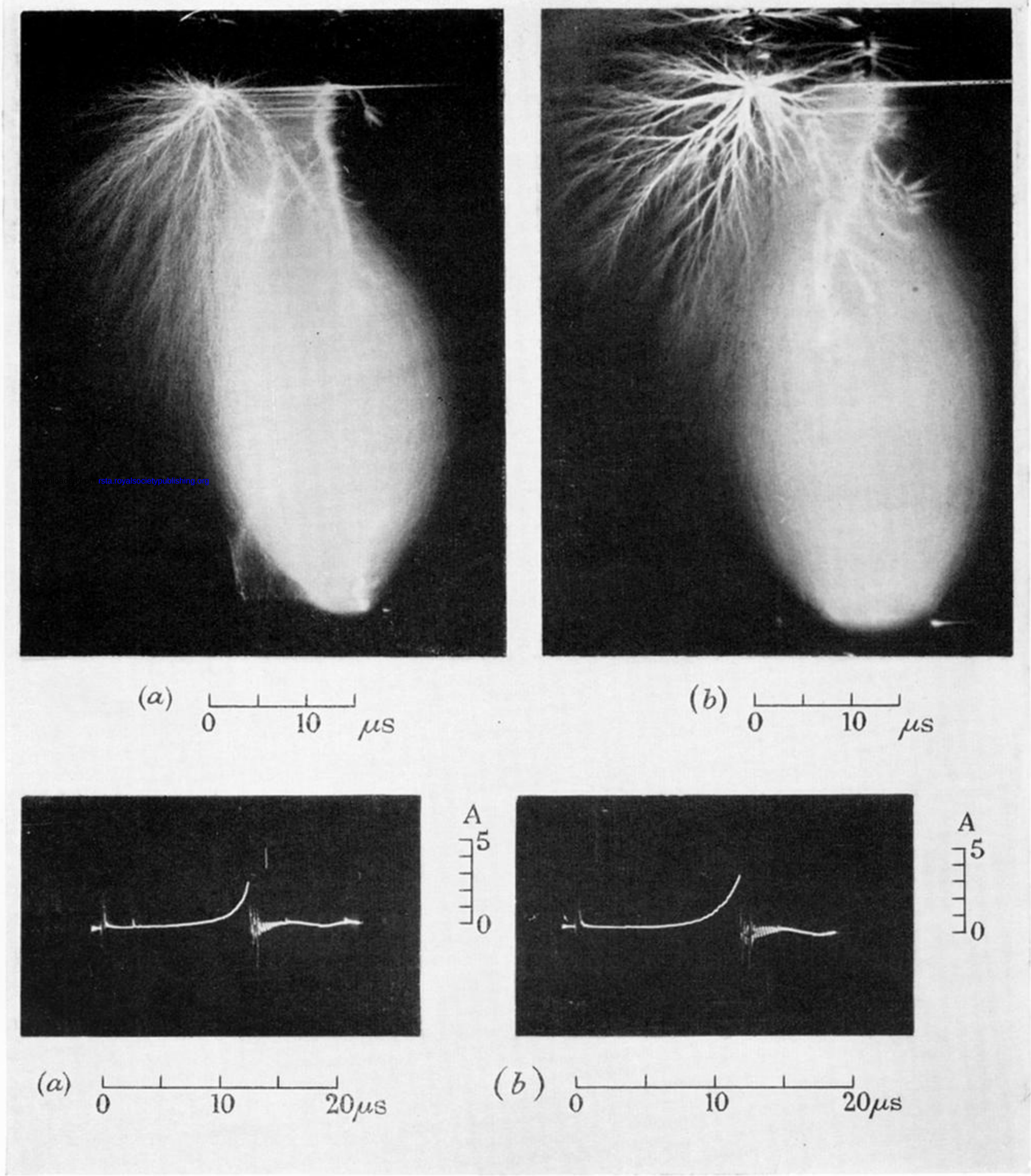

FIGURE 14. Time-resolved photographs of arrested breakdown in 80 cm rod/sphere gaps; wave shape 0·50/2000 μs. (*a*) 12·5 cm diameter sphere, 480 kV crest voltage; (*b*) 25 cm diameter sphere, 460 kV crest voltage.

IGURE 15. Time-resolved photograph of arrested breakdown in a 75 cm diameter sphere/rod gap at 900 kV crest voltage; gap spacing 65 cm; wave shape 0·50/2000 μs.